DETAILED NEW TABULATION OF ATOMIC FORM FACTORS AND ATTENUATION COEFFICIENTS IN THE NEAR-EDGE SOFT X-RAY REGIME (Z = 30-36, Z = 60-89, E = 0.1 keV – 8 keV), ADDRESSING CONVERGENCE ISSUES OF EARLIER WORK

C. T. Chantler,

School of Physics, University of Melbourne, Parkville, Victoria 3052, Australia

ABSTRACT

Reliable knowledge of the complex X-ray form factor (Re(f) and f″) and the photoelectric attenuation coefficient σ_{PE} is required for crystallography, medical diagnosis, radiation safety and XAFS studies. Discrepancies between currently used theoretical approaches of 200% exist for numerous elements from 1 keV to 3 keV X-ray energies. The key discrepancies are due to the smoothing of edge structure, the use of non-relativistic wavefunctions, and the lack of appropriate convergence of wavefunctions. This paper addresses these key discrepancies and derives new theoretical results of substantially higher accuracy in near-edge soft X-ray regions. The high-energy limitations of the current approach are also illustrated.

The associated figures and tabulation demonstrate the current comparison with alternate theory and with available experimental data. In general experimental data is not sufficiently accurate to establish the errors and inadequacies of theory at this level. However, the best experimental data and the observed experimental structure as a function of energy are strong indicators of the validity of the current approach. New developments in experimental measurement hold great promise in making critical comparisions with theory in the near future.

Key Words: anomalous dispersion; attenuation; E = 0.1 keV to 8 keV; form factors; photoabsorption tabulation; Z = 30 – 89.

Contents

1. Introduction and importance of form factors

The complex form factor f is the fundamental parameter for all optical devices. It specifies refractive indices, permittivities, scattering and attenuation coefficients, and hence the critical properties for mirrors, lenses, filters and coatings. At higher (X-ray) photon energies, the form factor becomes accessible to theoretical prediction on the basis of atomic physics and the atomic form factor.[1]

In the X-ray energy range covered herein, the primary interactions of photons with atoms are photoabsorption and coherent (elastic) scattering. Inelastic (Compton) scattering becomes dominant for all elements as the higher γ-ray energies are approached. For light elements, this transfer of dominance occurs at much lower energies (for hydrogen the inelastic component dominates above 3-5 keV). Additional nuclear scattering and absorption occurs above MeV energies, including pair production and Delbrück scattering from the nuclear field; and nuclear resonant processes (such as nuclear Thomson scattering).[2] For XUV photons below the energy range of this paper, lattice phonon absorption, delocalized plasmon excitation, excitons and dipole resonances may appear.[3] Although these remain qualitatively identifiable as photon interactions with bound electrons, it is misleading to attempt to identify them with atomic orbitals or isolated atoms.

In the intermediate energy range, typically from 0.01-0.1 keV through to 80-800 keV, the interaction of the incident photon with the electrons - i.e. with the bound atomic orbitals - without production of secondary x rays of reduced energy, is the dominant process. The

photon is then either scattered without altering the internal energy of the atom, or it is fully absorbed. This absorption is usually into a single atomic orbital, with a consequent ejection of a photoelectron and production of a singly-ionised species.

Photoabsorption and (Rayleigh) scattering are both described by the structure factor F of the material in condensed or gas phase. Diffracted intensity or coherent scattering is a complicated function of F, but for weak reflections is linear or quadratic in F. Equally, transmission through a bulk material is a complex function of F but local attenuation is a relatively simple function of the imaginary component of F.[4,5]

This is well known in the crystallographic community and is used extensively in the multilayer community at lower energies.[6,7,8] The structure factor for a given reflection (denoted *hkl* from the Miller indices) is a sum over the atoms in the appropriate lattice (for a crystal) of the atomic form factors or the X-ray scattering factors f_j of the j^{th} atom:

$$F(hkl) = \sum_j f_j e^{-M_j} e^{2\pi i(hx_j + ky_j + lz_j)}, (TDS = 0) \qquad 1$$

where thermal diffuse scattering is neglected, M_j is the thermal parameter for the given temperature, reflection and atom, and the location of the atom in the unit cell is given by (x_j,y_j,z_j). For an isolated atom or a single elemental lattice, a scaled atomic form factor may therefore be substituted for the structure factor.

At grazing angles of incidence with solids, photons interact with the surface, and the photoabsorption and reflection processes may be given by Fresnel equations (while still dominated by electron orbital interaction and governed by the structure factor and form factors).[9]

If the atoms in a condensed system may be considered to scatter as dipoles (i.e. for low energies or small scattering angles) then the interaction of x rays with matter may be described using optical constants such as the complex index of refraction n_r or the complex dielectric constant $\varepsilon(E)$, which are related to the form factors by

$$n_r = n + ik = \sqrt{\varepsilon} = 1 - \delta - i\beta = 1 - \frac{r_e}{2\pi}\lambda^2 \sum_j n_j f_j \qquad 2$$

where n_j is the atom number density and r_e is the classical electron radius.

2. Form factors and standard definitions

The (X-ray) atomic form factor f is the resonant scattering amplitude of X-rays by charge (primarily electron) density. Using standard conventions in the X-ray regime, we also consider the imaginary and real components of the form factor separately, and separate three contributions to the real component. The real component Re(f) is composed of: the 'normal' coherent scattering factor f_0, depending upon the photon angle of scattering θ via the momentum transfer

$$q = |\mathbf{K}-\mathbf{K}'| = 4\pi \sin(\theta/2) / \lambda, \qquad 3$$

with λ in e.g. Ångstroms; the 'anomalous' scattering factor f' (depending on X-ray energy E and the atomic number Z); and the small nuclear Thomson term f_{NT}.[10,11] f' can also be expressed in terms of a small relativistic correction term f_{rel}, Z and the function f_1 often used to characterise these form factors:

$$\mathrm{Re}(f) = f_0 + f' + f_{NT}, f' = f_1 + f_{rel} - Z \qquad 4$$

$$f_0(q,Z) = 4\pi\int_0^\infty \frac{\rho(r)\sin(qr)r^2 dr}{qr} \qquad 5$$

The angular factor f_0 is identical to the values f(q) or F(x,Z) given in Hubbell et al. (1975), Hubbell and Øverbø (1979) and Schaupp et al. (1983) and use q instead of x, with $x=q/4\pi$.[12,13,14]

$$f'(E,Z) = f'(\infty) - \frac{2}{\pi} P\int_0^\infty \frac{\varepsilon' f''(\varepsilon')}{E^2 - (\varepsilon')^2} d\varepsilon' \qquad 6$$

The imaginary component Im(f) = f' is directly related to the atomic photoabsorption cross-section given as τ_{PE} or σ_{PE} in different references:

$$\mathrm{Im}(f) = f''(E) = f_2(E) = \frac{E\sigma_{PE}(E)}{2hcr_e} \qquad 7$$

Fundamental constants and conversion factors are given in Ref. 15. Conventionally, the total interaction cross-section σ_{tot} is represented as a sum over the individual photon interaction cross-sections:

$$\sigma_{tot} = \sigma_{coh} + \sigma_{incoh} + \tau_{PE} + \kappa_n + \kappa_e + \sigma_{p.u.} \qquad 8$$

These cross-sections would conventionally be given in barns/atom. This would be directly related to the linear attenuation coefficient μ in cm^{-1}, and the mass attenuation coefficient in cm^2/g. The mass attenuation coefficient is conventionally given by the symbol $[\mu/\rho] = \sigma/uA$, where σ is the cross-section in barns/atom, u is the atomic mass unit, and A is the relative atomic mass of the target element. Coefficients for converting between these units are given by many authors (see the table header in section 12).[16]

This paper develops the approach covered in Chantler (1995)[16] and makes extensive reference to this earlier work, which will therefore be denoted in what follows as C95. Table I summarises the type of use to which this tabulation (and that of C95) may be put. It summarises the typical equation to use (with reference to column headings in the current tabulation) and gives the author's current personal recommendation of a useful or appropriate reference for additional information or coefficients as might be needed.

3. Concerns with standard conventions

Coherence of cross-sections: In Equation 8, σ_{coh} is the cross-section for coherent or Rayleigh scattering but is not always coherent. In other words, the complex Rayleigh amplitude for adjacent atoms does not necessarily add in phase, but may randomly superpose. This component represents the elastic scattering contribution to the interaction coefficient. It relates directly to the structure factor F. The structure factor depends on the material under observation and the crystallographic arrangement of atoms, and hence on both the real and imaginary components of the atomic form factor. For an isolated atom or elemental metal, the total elastic scattering of a material is dominated by the real component of the atomic form factor Re(f).

The 'incoherent or "Compton" cross-section' σ_{incoh} is likewise not always incoherent but represents the inelastic scattering contribution to the total interaction coefficient. This also depends upon the atomic form factor. The atomic photoabsorption cross-section τ_{PE} or σ_{PE} is directly related to the imaginary component of the form factor.

Simple addition of cross-sections: Simple addition of cross-sections from scattering and photoabsorption depends on the relative phases of scattered waves being incoherent, and may in some cases be quite inappropriate. In general the amplitudes should be summed including any relative phases. However the simple summation of the cross-sections represents a common and often very good approximation.

Contributions of high-energy terms in the medium-energy X-ray regime: The remaining terms in Equation 8 represent large contributions only for MeV energies and above, and as such are not the concern of the current discussion. They represent the pair production cross-section in the nuclear field (κ_n), the pair production cross-section in the atomic electron field (or triplet cross-section, κ_e), and the photonuclear cross-section $\sigma_{p.n.}$. An excellent review of these cross-sections is given elsewhere.[2] Below MeV energies all interaction coefficients depend directly and implicitly upon the real and imaginary components of the atomic form factor. The graphs below depict the mass attenuation coefficients and the values of the form factors themselves, since it is critical to present quantities in use but also the fundamental parameters underlying the used quantities.

Dependence of f′ and f″ on angle: There have been concerns regarding a possible angular dependence (or scattering vector dependence) of the anomalous dispersion (i.e. energy-dependent) components f′ and f″ of the form factor (Equations 4 and 7). The current status of this query is well represented by Creagh and McAuley, who summarise that there is no dependence of either quantity upon scattering vector.[17] Hence all angular dependence of the form factor for an isolated atom is contained in f_0.

The justification for the separability of the angular and energy-dependent components as given in Equation 4 is a related issue. If the two dependencies upon angle (in f_0) and energy

(in f′) are truly independent, then the components are clearly separable. However, it has been argued that this separation may not be valid for large energies and large momentum scattering vectors.[18]

Because of this, some authors define a modified form factor MFF (g) and anomalous scattering factors (g' and g'').[19] This formalism appears useful for MeV energies, but not relevant for the current discussion (the differences for even 500 keV energies are unobservable).[20]

S-matrix and general formalisms: There has been much publicity about the value of recent S-matrix computations.[18,20,21] There is no doubt that higher order corrections, particularly relating to the relativistic correction factor, are important and observable in principle. However, it is often not realised that the relativistic formulations of Cromer and Liberman[22,23,24,25] (and most derivations since) are based on the following S-matrix (or *scattering matrix*) equations for the superposition of the final states f (including ionized atoms, excited states, and elastic and inelastic scattered states) in a transition from the initial state i:

$$|\psi\rangle = \sum_f |f\rangle\langle f|S|i\rangle \qquad 9$$

$$S_{fi} = \delta_{fi} + 2\pi i\delta(E_f - E_i)T_{fi} \qquad 10$$

The scattering amplitudes T_{fi} in general are complex.[26,27] Most investigations have been restricted to coherent, forward scattering, and where changes in photon polarisation do not occur.

All general theories make the isolated atom approximation and the IPA (independent particle approximation). Any variation between computations based on these theories are due to other limitations, not to the use of isolated atom or IPA. Because of these assumptions, experimental work relating to solids may well yield very different near-edge structure and hence be unable to be compared to theory. In some cases, this gives significant variation between one experiment and another. The comparison of different theoretical and

computational schemes within these assumptions is unaffected by these solid state effects; and the conclusions below are largely independent of these concerns.

These approximations are usually combined with the electric dipole approximation to yield final computable results. In this sense all computations have made the same broad approximations. As seen below, most limitations can be attributed to convergence problems rather than to higher-order corrections.

4. Reliability of Experimental and Theoretical Results

This paper addresses a key theoretical issue behind this dilemma, focussing on the soft X-ray near-edge region. We derive new results based on the formalism of C95. We primarily compare our new theoretical results to those of C95 and Refs 28 and 29, because of the detailed and extensive discussion of these references over the last few years. A moderately detailed discussion of databases of Henke et al., Cromer and Liberman[25], and Brennan and Cowan[30] has been made earlier in comparison to C95.[1,31]

The primary experimental references for comparison in this paper will be Henke et al.[32,33] and those contained in Saloman, Hubbell and Scofield.[34] Compilations of experimental data for photoabsorption and total cross-sections are widespread[34], particularly for common elements over the central X-ray energies. These are particularly useful in evaluating the reliability of a particular measurement, or the difficulty of an experiment in a given energy regime. The range of the imaginary coefficient in such compilations often varies by 10% to 30%. This implies in general that claimed experimental accuracies of 1 % - 2 % are not reliable. The effect of a 10% error is equivalent to a 10% error in the thickness of the sample, or a 10% error in the exponent of the probability of photoabsorption through a sample.

The second primary source for an experimental best-fit line is given by the Centre for X-Ray Optics, Lawrence Berkeley Laboratory.[32,33] A recent successor in this series is presented by Cullen, Hubbell and Kissel,[35] but we do not discuss it further in the current context. These references present experimental-theoretical syntheses for the complex form factor in the softer X-ray regime. As a weighted evaluation of experimental data, they are extremely useful. However, no variation or error bar is associated with this single fit, and in

soft X-ray regimes, near-edge regimes and other areas the result may be in sharp discrepancy with theory and expected results, or with the best available data. Observed deviations lie at the same 10% - 30% level as the variation of less critical compilations.

For medical and diagnostic applications, reliance on either theory or experiment is dangerous: an 'ideal' procedure is to measure relative fluxes of energy distributions in situ, with and without filters, as they would be used in practice. This then ignores the relative significance of scattering, absorption, harmonic contamination and divergence effects, and yields a purely empirical calibration subject to the detector calibration itself. The danger of this approach is that lack of subsequent control of flux distribution with angle and energy, and of the orientation and uniformity of filters and optical elements, will lead to arbitrary and potentially severe changes (over time, or between exposures) in administered doses or derived structural distributions.

Given this situation, it is sensible to turn to theoretical computations. One of the most recent and comprehensive theoretical approaches was developed to explicitly eliminate these difficulties (C95). Useful recent general reviews of other theoretical and experimental compilations are given by Hubbell[36] and Creagh and McAuley.[17] These also discuss scattering contributions which are not the primary concern of this paper.

Comparing the new theoretical approach uncritically with other commonly used theoretical references[28,29,34] reveals surprising variation and uncertainty in the theory. Many references have been made to Scofield theory in unrenormalised and normalised forms, and we discuss some of the variations between these two results. Scofield presents only atomic photoabsorption cross-sections, τ_{PE}, so this discussion will be limited to the imaginary component of the atomic form factor. The real component will be discussed for comparison to Henke et al.[33]

It is difficult to accurately assign uncertainty to theoretical results, and the uncertainty varies dramatically across energy ranges for well-defined reasons. A number of authors give useful estimates based on convergence criteria,[28] on self-consistency or consistency with experiment,[34,4] or on a combination of these criteria (C95). A figure of 0.1% to 1% is often

quoted away from edges and in the medium energy range. This paper highlights and addresses the largest apparent single source of discrepancy currently observed.

5. General discussion of recent issues, and a summary of earlier issues

Hydrogen: C95 uses a simplified approach to give the form factor for hydrogen itself. This is extrapolated to high energies, and it may be noted that at very high energies there is an approximation error for the result for a single isolated hydrogen atom. The primary purpose of that tabulation (and the current work) is to address the need in crystallographic and synchrotron communities for accurate form factors for structural and other investigations. Hence the primary target lies over the range of X-ray energies. We are grateful to P. Mohr for raising this issue. Of course, for many investigations the form factor of bonded hydrogen is non-spherical and completely different from that for atomic hydrogen. In these cases a form factor for atomic hydrogen may be used to directly investigate the bonding patterns, and so the tabulated values remain useful. However, it is worthwhile investigating the actual limitation of C95 across the range of tabulated energies. This is presented in Fig. 1, where a variety of models are given for the hydrogen atomic form factor. The Sauter relativistic Born approximation is actually very poor for X-ray energies, but indicates the asymptotic limit at high energies.[37] This functional dependence is not observed in the earlier tabulation, and reference should be made to other sources listed here for energies above 433 keV.

Henke et al. (1988) covers a very restricted energy range, and the Sauter formula (e.g. Ref.37) only becomes a useful approximation at energies above 80 keV. With these two exceptions, all approaches appear very similar across several decades of energy and form factor. C95 is accurate to within approximately 2% up to 330 keV for an isolated hydrogen atom. The original tabulation presented results by extrapolation to 433 keV, where the relativistic high-energy correction to the simple result has a magnitude of 13-15%. Although this correction is beginning to be significant at this level, the magnitude of coherent and incoherent scattering dominates by seven orders of magnitude. Other comments regarding the utility of the earlier presentation were given in C95.

Singularities, Integration Precision, Interpolation: C95 detailed the correct approach to these issues, and discussed particular tabulations where problems of these types

have been noted earlier. The main problems related to the use of a relatively sparse set of values of f_2 as a function of energy, and the use of inappropriate formulae for the determination of the imaginary and real components of f from the atomic orbital wavefunctions. Both C95 and the current work are free from such problems.

Several approaches have major problems with extrapolation, interpolation and integration approaches to the determination of Re(*f*) and of Im(*f*). The work of Creagh and Hubbell[4] suffers from some generally minor limitations in this regard, and theory reported in Saloman, Hubbell and Scofield[34] is relatively free from these effects. This paper does not relate directly to regions of failure of extrapolation, integration or interpolation. However, the specific near-edge problems discussed below reveal new limitations which in some cases may be related to problems of extrapolation, depending on the computational approach used.

Comparison of recent tabulations for helium, Z=2: Helium is a near-perfect system for study. The gas is monatomic, the atoms are isolated and there are only two electrons (so the independent particle approximation (IPA) can be very good). Fig. 2 indicates that Scofield (unrenormalised)[34] deviates from experiment by generally 3-4 σ in the soft-to-medium X-ray regime, as opposed to C95, who lies within a fraction of σ deviation from experiment. C95 provided a simple computation of scattering coefficients to complement the more detailed computation of form factors contained therein.

If coherent scattering follows Bragg-Laue processes (such as for crystals and diffraction peaks) or Thermal Diffuse Scattering approximations (usually for crystals, but with explict alignment away from Bragg peaks) then the estimates of Chantler or Saloman et al. may be inappropriate and the actual scattering cross-section may be larger or smaller than that predicted, by an order of magnitude or more. However for isolated atoms such as helium, or for systems where the Rayleigh scattering approximation is good, the estimates of Ref. 13 (and herein) are expected to be good approximations to the experiment.

More detailed evaluation of scattering coefficients is given by Hubbell and Øverbø[13] (σ_{coh}), and Hubbell et al.[12](σ_{incoh}), tabulated in Ref. 34. Use of these (generally more

accurate) scattering coefficients with the attenuation coefficients of C95 yields very good agreement with the precision experiment of Azuma et al.[38]

The discrepancy shown in Fig. 2 is primarily due to the use by Scofield of Hartree-Slater orbitals, hence omitting certain relativistic corrections. At some level, this limitation would be expected to yield lower accuracy than the self-consistent Dirac-Hartree-Fock approach (Ref. 16 and this work). The general approach for new theoretical work is certainly to use a Multi-Configurational Dirac-Hartree-Fock approach whenever possible, and this argues for the approach of this work rather than that of Ref. 34. The DHF approach more accurately incorporates relativistic effects which become more significant for higher Z elements.

For Z=2 to 54, Scofield provided estimated renormalisation factors to convert to values which might be expected from a relativistic Hartree-Fock model. The difference between renormalised and unrenormalised results vary from about 5% to 15% or more for lower energies or outer orbitals, so is very significant in the current discussion. There are other differences between Scofield and Chantler beyond simply the Dirac-Hartree-Fock versus Hartree-Slater approach. The exchange potential of the Chantler approach follows that of Cromer and Liberman (1981) and Brennan and Cowan (1992) and is quite distinct from the approximation used by Scofield. On this issue the preferred approach is not clear *a priori*.

In the context of Helium, application of renormalisation would improve agreement with experiment, but by only a fraction of a standard deviation, and hence would not resolve the discrepancy. This large and significant discrepancy is several σ, but only about 8 % – 10 % in magnitude. Other discrepancies for higher Z elements show discrepancies many times this value.

Much recent theoretical and experimental work has investigated helium, particularly in the VUV region. These extensive calculations offer improvements in precision, particularly in the energy ranges below 300 eV and above 300 keV, while having similar quoted precision in the central X-ray range. A review has shown consistency of recent detailed calculations by Hino[39] and Anderson and Burgdörfer[40] with C95 in the region plotted in Fig. 2.[41] This review also showed the consistency of experimental results of Samson et al.[42] with Azuma et

al. and the inconsistency of these results with Henke et al.[33] and Viegele et al.[43] Detailed investigations of sum rules by Berkowitz[44] has supported the approach of C95. Undoubtedly further theoretical and experimental work is needed, particularly for the high energy regions.

Causes of uncertainty near absorption edges: The above examples concentrated on regions where alternate theories claim convergence to 0.1% and hence can claim accuracies of 1%. However, the greatest discrepancies between these theories occur near edges, with deviations by factors of 5 or more between alternate results.

The cause of near-edge error in theoretical computations is often due to inadequate interpolation, extrapolation or integration methods, which introduce apparent oscillations or discontinuities into the data.[31] The cause of near-edge error in experimental compilations is often due to neglect of the edge region or smoothing through edge structure.[33] The cause of near-edge error in specific experiments is often due to the dramatic variation of form factor with energy, requiring both accurate absolute intensity measurement and also precision energy calibration.[45]

Assuming that these issues have been correctly addressed, theory will disagree with experiment near edges by large factors due to XAFS and related structure. This can reach a 200% discrepancy between IPA theory and a solid-state experiment.[17] Even if the experiment is performed on a monatomic gas, there may be pressure-dependent structure and other strong oscillatory behaviour near edges. Some of this structure (shape resonances and Cooper minima) may be qualitatively predicted by some theoretical approaches, but often the detailed experimental result will show significant quantitative discrepancy.[46]

The largest discrepancies between C95 and the Scofield theory are not due to any of these causes. C95 claims uncertainties of up to a factor of two (50%) in soft X-ray near-edge regions. Ref. 34 refers to 10% -20% discrepancies from experimental data in the medium-Z regime, which may be taken as an uncertainty estimate.

In most elements and regions, the near-edge variation falls within these error bars. This is illustrated for copper in Fig. 3. Such experimental data is not sufficiently precise to distinguish between these two theories, or even to observe edge structure which would diverge from Refs 32,33. Fig. 3 indicates the 1 keV lower limit of the range of Ref. 31. The

current result is slightly modified in the near edge region, but the accuracy here is not improved, the difference between the earlier result of Chantler and the current are within one standard deviation, and we do not present this in the following tabulation. A detailed experimental work claiming 4% accuracy has recently demonstrated good agreement of C95 with experiment and with Creagh and McAuley[17] for copper.[47]

Experimental data have large scatter and large uncertainties compared to the theoretical discrepancies discussed here, and hence cannot distinguish between the alternatives. This is generally true for this near-edge soft X-ray region, and has made comparisons of theory difficult. Figure 3 also plots experimental data plotted for f_2 rather than μ/ρ. This involves a straightforward scaling of attenuation data and subtraction of scattering contributions to attenuation cross-sections. The coherent and incoherent scattering functions contribute a maximum of 1.5% in the region tabulated, and a maximum of 0.2% in the regions near edges. The uncertainty in this subtraction should generally be less than 0.2% and hence will not add to the experimental uncertainty. The experimental references in the figures are taken from the comprehensive database of Ref. 31. Refs 48 indicate the range of references used in compiling Fig. 3, as a typical example.

6. Uncertainties near soft X-ray LII, LIII, MIV, MV edges, and the reason for the new tabulation

In the region 1 keV – 2 keV for particular edges in medium or high-Z elements, enormous discrepancies are observed between the theoretical treatments of C95 and Ref 34. The first occurrence of this effect in C95 is illustrated in Fig. 4 for Zn, Z=30. On a log scale the variation is suppressed and may be overlooked; but on this linear scale the enormous peaks and oscillatory behaviour of C95 is unmistakeable. This is *not* due to XAFS or any such near edge oscillation. Despite the large magnitude of this discrepancy, experimental results are still generally unable to discriminate between the two theories and Henke (1988 and 1993).

Relative to appropriate high-energy theory, which would yield well-defined edges and smooth behaviour for each orbital on a log-log plot, the results of C95 and Refs 32,33 and 34 are all in error. The structure from C95 could be interpreted as a sharp shape resonance, but it is a fictitious one.

This error arises from an accumulation of minor errors in inner shells and the electronic wavefunction distributions. Particularly for near-edge energies, these errors accumulate, which is a strong reason for the low accuracy claimed by theory in this region. The K shell (1s orbital) and LI shell (2s orbital) are usually accurately computed, and the form factors for these sub-shells are accurate; but the errors for LII and LIII (2p) are amplified, and also fall in increasingly difficult soft X-ray energies. Hence the wavefunction solution for the orbital radial electron density, which leads to the computation of the near-edge form factor, becomes unreliable and increasingly inaccurate. Similarly, the MI-MIII (3s, 3p) edges are well defined, but the MIV and MV (3d) structure is poor near the absorption edge.

For C95, this yields a sharp slope for the LII/III-edges for Z=30-36, and for the MIV/V-edges for Z=60-88. For Ref. 31, this effect appears periodically in a less well defined manner.

Within the convergence criteria for the DHF wavefunctions, this may be more or less difficult to address, depending upon the exchange potential and method used. In the case of C95, we have been able to retain the original formalism but simply to require a better and more uniform convergence in these regions.

When the wavefunctions of C95 are improved and this issue is addressed, we obtain the 'New' or 'Current Result' [Figs 3 et seq.]. These new results are tabulated for the regions of atomic number and energy where any significant imprecision was observed. The results of this work also appear to reliably obtain the theoretically expected IPA edge structure. The precision of these results is clearly dramatically improved; but the accuracy is still limited for the reasons discussed above. Hence we would claim no better than 20% - 30% accuracy in this region, even though in some cases experiment may agree to better than 10%.

This paper emphasises the results of this investigation for the imaginary component of the form factor. The same structures are seen on an expanded log plot of $[\mu/\rho]$ as illustrated by Fig. 5. Due to space constraints, we present plots of the real and imaginary components of the form factor for all energies and all atomic numbers affected, but we present $[\mu/\rho]$ only in the tables. As indicated in Eqn 7, there is a simple relation between the two.

The same qualitative errors in structure for f_2 or $[\mu/\rho]$ are transformed following Eqns 4 and 6 into qualitative errors in the structure of Re(f) as a function of energy, as indicated in Fig. 6. The result reported here is in better agreement with Henke et al.[32,33] than C95, and includes features for all edges. The most common spurious structural effects in Re(f) are seen just above the edge, where a spurious peak may appear, and in subsequent waves of dips and peaks extending up in energy for some keV or so. This same structure also leads to an accentuated minimum in Re(f) at the edge location, and also to an apparent decrease in Re(f) or f_1 below the edge, by perhaps 1 e/atom. These secondary effects are quite variable, depending on the nature of the approach to convergence of the wavefunctions. However, this seems to represent the most common signature in problem cases in C95.

The transform of the erroneous structure shows significant deviations from the new result, in some cases down to 100 eV. Hence the plots and tabulations cover regions down to 100 eV even though the error in convergence of f_2 only exists in the 1 keV – 4 keV region. By providing this full region, we allow the new tables to be continuous with the older tabulation of C95, so that a simple replacement of the new material for the old yields a smooth and continuous result. We have taken the opportunity suggested by colleagues to implement a finer grid spacing in this near-edge regime, simplifying any interpolation which may be applied to the data.

C95 stated low energy, high energy and near-edge limitations of this tabulation, which also apply to this current work. The main difference is the new precision in the computation of soft X-ray near-edge regions. However, we tabulate these estimates of precision in Table II, and give an indication of the effects which limit the accuracy in these regions. Two types of inaccuracy may be identified. The first listed is the estimate of convergence precision (intrinsic to the computation), while the second is an estimate of additional structure (such as XAFS or solid state effects) in particular applications.

7. Comparison of agreement of earlier tabulations with the New Result

The worst cases of this convergence error in C95 are represented by Zn Z=30 and Pm Z=61 [Fig. 7]. The imprecision of theory increases towards lower energies below the edge. A rough estimate of the imprecision for experiment, Henke,[33] C95 and this work is given by

the difference between Henke and C95. Hence this uncertainty reaches 50% below 300 eV, and lies around 10% at about 600 eV. The uncertainty in theory within 10% of the edge is estimated to be about 10%, so between 600 eV and 900 eV we might expect agreement of theoretical approaches at the 3% level. The discrepancy with Henke lies at the 10% level which in this region we attribute to solid state structure or to the synthesis used by Henke.

In the high- energy region convergence of theory would expect a 1% accuracy, but discrepancies of 6% are observed. These areas must be the subject of future experiments in this field.

The convergence errors of C95 near the edge represent 1.5 σ errors, where σ is estimated as 50%, as stated earlier. In these and similar cases the Scofield result yields 80% and 220% errors near the edge (or 4-5 σ errors); conversely, C95 yielded maximum 68% and 87% errors respectively at the same locations. We assume that the cause of the Scofield discrepancies lie in the same problem regarding the electron distribution. This will be affected by the formalism used to derive the wavefunctions. The C95 convergence errors tended to be extended over slightly larger energy ranges (i.e. 40-50% versus 20-30% above the edge). For Z=61, [Fig. 7]

Henke[33] displays 30% discrepancies in the near edge region. Henke includes a weighting for a theoretical prediction, but may be affected more by the scatter of available experimental results, or by the Z-interpolation scheme used. Figs 8 and 9 illustrates these percentage deviations explicitly compared to this work (which also has an uncertainty, but yields a correct IPA structure).

As stated, usually the experimental data is inadequate to make a critical comparison of C95 or of the current work with respect to other databases. A nice comparison is however given by the noble gas Kr, Z=36 (Fig.10).[49] Here the structure suggested by C95 is clearly incorrect, although the theoretical uncertainty was almost equal to the difference between C95 and experiment. The structures of Henke[33] and Scofield[29] are also seen to be in error, particularly for the L III edge region, although for krypton this maximum error is 50% rather than the larger error of C95. The experimental data set plotted here is quite dated, and we estimate experimental uncertainties to be ±4%. The precision appears to be better than this,

and possibly approaching the 1% level. This is therefore a good data set, and there is also the advantage of this refering to a monatomic gas, so that the independent particle approximation should be valid.

Other experimental data is plotted in the tabulation. Results for Yb (Z=70), Lu (Z=71) and Ta (Z=73) suggest a smoothed M_V edge structure, although this may be partly due to detector and monochromator resolution.

Current experimental data for rhenium (Z=75), gold (Z=79), lead (Z=82) and bismuth (Z=83) also give strong evidence against the oscillation of C95. In particular, data for gold (Z=79) and lead (Z=82) appear to favour the current work rather than Henke[33] and Scofield[29], certainly in the near-edge region for the M_{IV}/M_V edges. The predicted structure matches up very well with the current result, as opposed to alternatives. There is some indication of M_V smoothing, which may also be due to detector and monochromator resolution. Scattering contributes to the experimental data at the 0.1% to 0.25% level. These plots also show some absolute offsets at the 1-2 σ level, where σ is given by experiment. There is strong motivation for high accuracy experiments to address these sorts of discrepancies and to reduce the experimental uncertainties by a factor of three or so.

A confirmation that the region of interest has been fully addressed is given by the result for Z=37 (Rb) in Figs 11 and 12, and by the result for Z=59 (Pr) in Figs 13 and 14. Here the revised approach is indistinguishable from the earlier result, and the signature of the previous lack of convergence is absent. Figs 13-14 show all L and M edge regions for completeness. Hence the earlier tabulation is not reproduced for the elements lying between these in the periodic table.

Neodymium Z=60 and actinium Z=89 are included in this tabulation. Although the results for Z=89 was not obviously affected by the earlier lack of convergence, the new results show a very minor variation which is therefore also presented.

A recent experimental programme by Chantler et al.[45] is proceeding to address the experimental variation in the literature, by measuring attenuation coefficients to much better than 1% over central energy ranges for important elements. Other work is also in progress by several experimental groups. A number of detailed XAFS studies have been made, which

often show high resolution relative structure but without an absolute calibration to compare directly to theory. Of course, the near-edge region of direct relevance here is also strongly affected by XAFS, which are intrinsically solid state interactions not represented in the current series of tabulations. The main exception to this rule are the noble gases He, Ar and Kr as discussed above.

All these experimental programmes hold the prospect of reducing the experimental uncertainty to much less than the theoretical variation, which will allow much more critical investigation of atomic and solid form factors. A number of detailed theoretical issues including the near-edge 'offset' from IPA theory will then become accessible to investigation.

Even where experimental accuracy is inadequate to discriminate between theoretical alternatives, the anticipated atomic edge structure is reasonably well represented by the new results tabulated below, and differs from that of all of the earlier tabulations represented in the plots. The tables and plots show that the experimental structure represented by the experimental data for krypton, Z=36, and other elements support the edge structure of this work rather than that of earlier references.

8. How to use these tables

These tables should be combined with the tables of C95 unless the full range of interest is covered in the tables here. Then the tables provide f_1 and f_2 form factors and $[\mu/\rho]_{PE}$ for all elements up to Z=92 from 0.001 – 0.01 keV to 1000 keV.

Values for f_1, f_2 or $[\mu/\rho]_{PE}$ should be extracted from the tables for the given element(s) and energies required. Linear interpolation of f_1 should be adequate, while linear log-log interpolation of f_2 or $[\mu/\rho]_{PE}$ should be adequate on this scale, if required.

The energy range covered exceeds that for normal X-ray diffraction and crystallography studies but allows limitations and specialised experiments to be investigated with reference to updated and corrected theory. Discussion of solid target effects, correlation, nuclear resonances and uncertainties should be noted carefully in applications below 1 keV or above 100 keV.

The tabulation provides a sufficiently fine grid with accurate atomic edge structure to allow such experiments as DAFS (diffraction anomalous fine structure) to investigate fine structure and spatial distribution of atoms and electrons within materials.[50] Multilayer diffraction experiments may be pursued at lower energies in an analogous manner.

8.1 Computation of form factors for forward scattering

Equation 4 should be used to obtain f' using the negative value of f_{rel} as included at the top of each table for each element. For comparison to old data or computations, the value corresponding to Ref. 6, denoted H82, may be used (following Cromer and Liberman but omitting the Jensen energy-dependent correction).[22-25,51] More recent work has suggested not only that the Jensen term should be omitted but also that the appropriate relativistic correction is 3/5ths of the Cromer-Liberman value. [52,4] This latter value is denoted 3/5CL at the top of each table for each element. Likewise, the nuclear Thompson term (also negative with respect to the atomic phase) is provided at the top of each table for each element.

For comparisons to other results in the forward scattering limit where the momentum transfer q=0, the value of f_0=Z may be used and the real and imaginary components of f are then fully defined. As an example, the forward scattering limit for copper at 10.32 keV, in electrons per atom, is f= Re(f) + i Im(f) = 28.07(28)-0.0876-0.000726 +i3.05(3). Clearly the uncertainty in the computation of f_1 dominates over the relativistic and nuclear Thomson corrections in most cases.

8.2 Computation of form factors for high energies and large momentum transfers

For large scattering angles it is necessary to use a more appropriate value of f_0 than f_0=Z, as may be gained from Refs 12,13,14,29 or 53. This is generally true for Bragg diffraction calculations. For example, metallic copper with a lattice spacing of 2d= 3.6150 Å will yield a momentum transfer $q=4\pi/2d=3.476$Å^{-1} or x=0.2766Å^{-1}. [The maximum momentum transfer for a back-reflected beam at this energy would be $q=4\pi/\lambda=10.4598$Å^{-1} or x=0.8324 Å^{-1}.] We note that for q=0 the tabulated values are exact, but uncertainties quoted in tabulations of f_0 refer to 1%-5% of the total, which would predict 0.29 e/atom uncertainty for q=0. Nonetheless, we use 1% here and add the uncertainties in quadrature. Then use of Ref. 53 (for neutral copper atoms) gives f_0=20.713 e/atom for the Bragg reflection, or f=

Re(f) + i Im(f) = 28.07(28)-0.0876-0.000726+[20.713(207)-29] +i3.05(3) = (19.69±0.35) +i(3.05±0.03) e/atom.

8.3 Computation of structure factors

Then the composition and arrangement of the material may be used as indicated in the introduction to provide structure factors (Eqn 1), refractive indices (Eqn 2), and Fresnel coefficients (Eqn 54 of Ref. 33, for example), together with scattered, diffracted or transmitted intensities. More complex formula may be found in the relevant literature, allowing for thermal diffuse scattering, orientation effects, and the zeroth order reflection in particular.

8.4 Crystallography (diffraction)

For a general diffraction profile calculation, there is usually a need to consider at least two waves: the incident wave and the corresponding attenuation of this wave (represented by the zeroth order diffraction, the Fresnel equations for the interface, or equivalently the q=0 forward scattering component) and the nearest Bragg-diffracted wave. There is often the need to consider multiple-beam diffraction, and in general the solution to a particular problem may require a dynamical theory of diffraction applied simultaneously to each of these waves. As a brief summary of some possible relevant formulae and applications, we refer to Refs 5,54,55,56 (curved crystal diffraction), Refs 6,7,8,57 (single layer or multilayer reflectivities and Fresnel equations), Refs 58,59 (flat perfect crystals), and Ref. 60 (general discussion of many related issues). This is not intended as a complete list, but as a useful guide.

8.5 Electron density studies

As a simple extension of Eqn 1, we note the field of difference density mapping uses the following Equation for the exploration of bonding patterns:

$$\Delta\rho(x,y,z) = \frac{1}{V}\sum_h \sum_k \sum_l \Delta F(hkl) e^{-2\pi i(hx+ky+lz)} \qquad 11$$

8.6 Computation of sum rules

Sum rules have been discussed and investigated, particularly at relatively low energies. Good recent examples are given by Berkowitz,[44,61] Barkyoumb and Smith,[62,63] and others.[41,64] Such studies serve to highlight relativistic corrections to form factors and to

confirm self-consistent tabulations. The relevant formulae are given by the high-energy limit of the Kramers-Kronig relation, and by other energy moments involving the form factors.[65]

8.7 Computation of scattering cross-sections

The structure factors may be used to compute differential or integrated coherent and incoherent scattering cross-sections directly, rather than using the integrated sum given in the tables, which assumes Rayleigh scattering for the coherent component. Standard formulae for the Thomson scattering of unpolarised incident radiation, the intensity of Rayleigh (elastic, coherent) scattering, and the incoherent (inelastic) scattering are

$$I_e = I_0 r_e^2 \left[\frac{1+\cos^2\theta}{2}\right],\ I_{coh} = I_e\left(\sum_{j=1}^{Z} f_j\right)^2 = I_e f^2, \qquad 12$$

$$\text{and } I_{incoh} = I_e\left(\sum_{j=1}^{Z}(1-f_j^2 - \sum_{k\neq j}\int \psi_j^* \psi_k e^{iq\cdot r} d\mathbf{r})\right) = I_e S(q,Z) \qquad 13$$

In these equations, f_j is the form factor for an individual orbital, leading to the sum f for the atomic form factor. Corresponding integrated cross-sections, as presented in sum in C95, this work, and (for example) Refs 2 and 13 are given by

$$\sigma_{coh.Rayleigh} = \pi r_e^2 \int_{-1}^{1}\left(1+\cos^2\theta\right) f^2(q,Z) d(\cos\theta) \qquad 14$$

$$\sigma_{incoh.Compton} = \pi r_e^2 \int_{-1}^{1}\left(\frac{1+\cos^2\theta + \frac{k^2(1-\cos\theta)^2}{1+k(1-\cos\theta)}}{(1+k(1-\cos\theta))^2}\right) S(q,Z) d(\cos\theta), k = \frac{\hbar\omega}{mc^2} \qquad 15$$

where the large bracketed factor represents the recoil process for a free electron as given by the Klein-Nishina formula[66] and the binding effects are included by the incoherent scattering function I(q,Z) or S(q,Z).

However, for N atoms in a unit cell of volume V_c, the coherent scattering in a Bragg reflection should be summed in phase to give $I_{coh,H=hkl} = I_e F_{H=hkl}^2$ for the structure factor F from Eqn 1. Use of the structure factor F then leads to (coherent) Bragg-Laue diffraction, with m_H the multiplicity of the hkl reflection and d_H the spacing of the hkl planes in the crystal yielding

$$\sigma_{coh.BL} = \left(\frac{r_e^2\lambda^2}{2NV_c}\right)\sum_H\left[\left(\frac{1+\cos^2\theta}{2}\right) m d |F|^2\right]_H \qquad 16$$

This is a much larger value than the Rayleigh computation, and assumes alignment of the Bragg planes near a Bragg condition. The corresponding thermal diffuse scattering approximation assumes the scattering crystal is explicitly misaligned from any Bragg conditions, and leads to a much lower cross-section

$$\sigma_{coh,TDS} = \left(\frac{r_e^2\lambda^2}{2NV_c}\right)\sum_H\left[\left(\frac{1+\cos^2\theta}{2}\right)md|F|^2\left\{1-e^{-2M}\right\}\right]_H \qquad 17$$

$$\text{or } \sigma_{coh,TDS} = \pi r_e^2\int_{-1}^{1}\left(1+\cos^2\theta\right)f^2(q,Z)\left\{1-e^{-2M(q)}\right\}d(\cos\theta) \qquad 18$$

Corresponding formulae may be found in Refs 2,13,20 and 60 for differential cross-sections. Because these various formulae have significant energy and angular dependence, and vary dramatically from monatomic gas to aligned or misaligned solid, it is often advisable to compute the scattering cross-sections directly rather than to use a simple approximation. However, the full version of the incoherent cross-section cannot be computed from the data in C95 or this work, because we do not present the orbital wavefunctions needed to compute the interference term of S(q,Z). It is however possible to compute the coherent cross-sections in any approximation, and to compute the estimates of S(q,Z) omitting that last term. For most low or medium-energy purposes this is quite adequate, but we also present the sum of coherent and incoherent cross-sections under the assumption of Rayleigh scattering, in the tabulation.

8.8 X-ray Attenuation [Medical imaging, transmission studies]

For filters or filter materials, the photoelectric attenuation coefficient is provided in order to compare to appropriate experiments or to allow for objects in a beam-line. The conversion to this from f_2 in appropriate units is provided at the top of the table. Use of barns/atom is also common, and the conversion factor for this is also provided. Often this column is not measured, and only the total observed mass attenuation coefficient

$$[\mu/\rho]_{TOT}=[\mu/\rho]_{PE}+[\sigma/\rho]_{coh}+[\sigma/\rho]_{incoh} \qquad 19$$

is observed. These latter two coefficients are angle-dependent and may in part be determined from appropriate structure factors for a given crystal orientation as described above. However a column is provided for the sum of these two latter coefficients in an average-over-angles for an atomic scatterer.[43,67] These references should be consulted for

details concerning the approximation involved, although the column in the current tabulation is a new computation of the sum (following C95). The main assumption is that Bragg-Laue peaks and troughs are avoided, or that the material is randomly oriented and preferably mosaic. If this is not true, it may be necessary to compute the dynamically diffracted intensities from the structure factor rather than rely on the approximation. However, simply summing these two columns allows the comparison of theory to experimental attenuation data. For most regions of interest for medical imaging, this is an adequate approximation. The accuracy of the scattering coefficients (within the Rayleigh approximation) is of order 5%.

8.9 [High-energy] Radiation Shielding

For high energies (the transition depends upon Z), the coherent and incoherent cross-sections dominate over the photoelectric cross-section. In this region the scattering coefficients of Refs 2 and 13 are recommended as a possibly higher precision computation. At this point the experimental evidence on this point is inconclusive, but we do not claim any higher accuracy than 5% for these scattering estimates. At high energies there may also be interference between the photoeffect and coherent cross-sections, in which case the current tabulation is important in identifying such effects but not in computing them.

At 1 MeV energies and above, (or at γ-ray resonances), nuclear physics dominates and we recommend inclusion of corrections by Hubbell et al.[12,13] for radiative and double-Compton contributions to incoherent cross-sections, reaching 1% at 100 MeV energies, and those of nuclear-field pair production κ_n beginning at $2m_ec^2$ = 1.022 MeV and becoming dominant around 10 MeV. Electron-field pair production (`triplet production') begins at 2.044 MeV and contributes above this energy at the 1% level for high Z elements but up to 10% for fluorine and 50% for hydrogen (or 1/(1+Z)). Nuclear photoabsorption consists of one (or a few) peaks (giant resonances) between 10-24 MeV of width 3-9 MeV, contributing up to 10% of the total cross-section in this region. Elastic processes include high energy Delbrück and dipole resonance scattering in addition to Rayleigh and nuclear Thompson contributions mentioned above.

8.10 VUV reflectivities and multi-layer computations

In addition to the discussions in Refs 6-8, relating to multilayer theory, experimental investigations in the VUV region suffer from the limited precision of theory (and of this current work). Our best recommendation regarding the estimation of either the magnitude of the form factor for an element in this region, or for a structural feature in this region, is to compare the results of the current approach to that of Ref. 33, and to treat the difference as an estimate of the theoretical uncertainty in the region. The major problems arise from valence shell correlations, and hence poor convergence of orbitals, and from correlated excitations, phonons and other solid state interactions. At the current time, we only present the results of C95 and this work as a guide in the region below 100 eV.

8.11 Individual orbital cross-section studies, and fluorescence yields

The column providing the photoabsorption coefficient for the K-shell only is included for two purposes. The first is that at high energies this is the dominant contribution to the total photoabsorption, and provides a guide for the local energy dependence of the cross-section. It serves as an illustration of the isolation of individual orbital cross-sections, particularly for higher energies.

The isolated K-shell cross-section is also important for experimental diagnostics and corrections. In particular, fluorescence yields from atoms are negligible for almost all orbitals except the K-shell, when compared to Auger and Coster-Kronig transitions. However, the fluorescence yield fraction for the K-shell is large, so the dependence of the cross-section upon energy is equally important. The qualitative result in an experimental ion chamber is significant - the fluorescent X-ray may escape from the ion chamber without conversion to (detectable) ion pairs. A more detailed discussion of this is provided elsewhere.[42]

8.12 Comparisons to literature

The plots provide comparison to the theoretical results of Scofield,[28,29,34] the experimental compilation of Saloman et al.,[34] and the experimental synthesis of Henke et al.[32,33] This is considered by the author to be the most useful and convenient comparison of current work in the literature. Scofield is often cited and the original stimulation for the preparation of this work was a comparison with that theory. The plots indicates limitations regarding restricted ranges and tabulation steps, shows good agreement over much of the energy range for many elements, and indicates regions of divergence, difficulty or concern. Some of these concerns have been addressed directly in this paper, while others remain. A

naïve statement of uncertainty in Henke or this work arises from the divergence between the two. This may relate to local structure, absolute values, or global structure. An alternate error estimate is provided in Table II.

8.13 Chemical Shifts

The edge energies used follow Ref. 68 are provided at the top of each table so that criticism (or experimental investigation) may indicate a shift of the local energy scale which *may* be appropriate in a specific material or experiment. This is not encouraged or recommended; nonetheless, it is provided as a statement of the assumptions and basis of the computation.

8.14 Electron form factors and scattering

Within the isolated atom approximation for spherically symmetric atoms, the electron atomic form factor is given by an analogue of Eqn 5, with the electron density replaced by the periodic potential $\varphi(r)$:

$$f^B(q,Z) = \frac{2me}{\hbar^2}\int_0^\infty \frac{\varphi(r)\sin(qr)r^2 dr}{qr} \qquad 20$$

Poisson's equation relates the potential and charge distributions, and leads to the Mott-Bethe formula for $f^B(q,Z)$ in terms of the X-ray atomic form factor $f(q,Z)$:

$$f^B(q,Z) = \frac{me^2}{2\pi\hbar^2\varepsilon_0}\left\{\frac{Z - f(q,Z)}{q^2}\right\} \qquad 21$$

On the basis of these formulae, numerous studies can be and have been conducted, and we refer simply to two summaries for elastic and inelastic scattering.[69,70]

9. Summary of uncertainties

f_2 and $[\mu/\rho]_{PE}$

Estimates of uncertainties are provided in Table II. Relative uncertainties in f_2 and $[\mu/\rho]_{PE}$ are identical. The accuracy of f_2 in this work and C95 in a central X-ray region well away from edges is estimated as 1%. This claim leads to significant discrepancies with other theory and experiment, which must be the subject of future investigation.

At low energies (especially below 200 eV) the uncertainty of C95 is very large and reaches 100%-200%. This is due to the dominance of non-IPA interactions in this region.

The best estimate of the accuracy of reported structure in this region (in C95) is given by comparison to an independent experimental or theoretical source, such as Henke et al.[33]

Accuracies below 1 keV reach a few percent or better in the absence of edge structure, and accuracies somewhat above edges are intermediate in estimated accuracy.

In the near-edge regions of direct concern to this work, the results of C95 should be replaced by the current tables in overlapping regions. Then the estimated uncertainty of f_2 in the combined tabulation (for energies and edges above 1 keV) is 20-30% compared to a monatomic gas form factor (i.e. ignoring the effects of solid state structure and XAFS, for example). The presence of molecular or solid state interactions can lead to dramatic excursions from theory for a monatomic gas in these regions, which can exceed 50% in extreme cases.

Energies

In this near-edge region the location of the edge is critical to a general comparison, and this work uses the same experimental edge energies as C95. They are usually in good agreement with experiment (say to a few eV) and with those listed for Ref. 29. However, there are exceptions to this as indicated in the plot for gallium, Z=31, where discrepancies might reach 100 eV. Some of these variations are due to experimental calibration errors or to chemical shifts of up to 10 eV. Others are not clear at this point, and we have preferred to be consistent with C95 than to alter any of these.

f_1-Z_{eff}

The precision of f_1 is dominated by that of f', so any percentage uncertainty should be expressed in terms of this or of f_1-Z. However, below an edge the orbitals do not contribute to f_2 and do not need to be computed for f_2 except for near-edge discrete transitions. Hence the effective Z is reduced. However, as seen for Nd, Z=60, and other elements, an error of f_2 at an edge can significantly affect the value of f' some order of magnitude below the edge. The typical ideal is represented by the results for krypton, Z=36, where an error (or uncertainty) in f_2 has lead to errors of some 50% for f' in the near-edge region, but has had no effect some factor of two in energy below the edge. Further, we find that at that point a factor of two in energy below the edge, the value of f_1 correctly represents the number of effective oscillators at this energy – i.e. 30 rather than 36 (for forward scattering). An error of

f_2 at a lower energy would therefore be expected to have an effect on the region of the edge (within a factor of two) at the 50% level, applied to f'-30.

C95 has discussed several types of error corresponding to 100%-200% errors in this value near edges. While this work is free of those errors, any computation of f' is extremely sensitive near edges to the sharpness of the discontinuity in f_2. As such there will remain significant uncertainties in the near edge region, of perhaps 50%. In any application of Re(f) away from forward scattering, the uncertainty in f_0 computations (or in f_0-Z) may be 1%- 5% and may dominate over the uncertainty in the anomalous dispersion f'.

f_{rel}

Because of the nature of the computation, the error in f_1 at very high energies can be very small and much less than 0.1 e/atom within the current formalism. This may compare with previously discussed limitations at the 1-3 e/atom level of some sources.[16] This is because f_1-Z becomes very small and indeed dominated by the relativistic correction f_{rel} and that associated uncertainty. We do not tabulate this uncertainty because the experimental evidence is usually limited by other uncertainties. An upper estimate for old sources of data is represented by the differences between the two values provided in the header of the tables for each element. This 'H92- 3/5CL' value is 1.09 e/atom for uranium or 0.002 e/atom for Z=6 (i.e. 40% of the dipole correction). However, we suggest as a lower estimate of uncertainty the difference between the results of Creagh[17,71] and Kissel.[72] This reaches 19% of the total relativistic correction for Z=90, or 0.3 e/atom, or 1% of the relativistic correction for Z=6.

$[\sigma/\rho]_{coh+inc}$

The column for Rayleigh scattering and incoherent scattering is of no value for angle-dependent studies (this should be recomputed as discussed above). It is also of little value in experimental comparisons of aligned or misaligned Bragg-Laue scattering, except to estimate the magnitudes of these processes (again, see the discussion of uses of this tabulation). However, it allows us to compute a total attenuation coefficient $[\mu/\rho]$ in the tables, and to point out the relative significance of isolated atomic scattering for each element at various energies. This is the prime use to which this column should be put.

The accuracy of this computation for scattering varies, and also improves for higher energies, but we estimate it to lie at the 5% level. This value is generally consistent with

discrepancies from Ref. 13 and 19. Ref. 11 claims to approach 1-2% in several regimes, but notes some particular deviations of 10% for heavy elements at 100 keV, for example.

10. Conclusion

Several generic difficulties with experimental and theoretical determinations of the atomic form factor in the X-ray region have been identified and resolved. We recommend intelligent application of a variety of the available experimental and theoretical sources, depending upon the user's purpose, and as summarised in Tables I and II, and section 8. Regions of solid state structure and XAFS limit the overall accuracy of such theoretical work unless explicitly modified to include such nearest neighbour effects, or comparison is made directly to monatomic gases. However, strong reasons favour use of theoretical sources at the present time for energies above 1 keV, for most applications. In this context, results based on Chantler (1995)[16] but with the current results presented here appear most reliable.

There are selected experimental data sets, which appear reliable, which suggest the accuracy of Chantler (1995) compared to e.g. Saloman, Hubbell and Scofield (1988). Both theoretical approaches had large uncertainties in the soft X-ray near-edge region for a range of elements, for well-defined reasons. The convergence error of Chantler (1995) was at all times within 1.5 σ. However, this still represented a large area of concern, particularly for present and future experimental investigations, even though it was often more accurate than Ref. 34. We have improved upon the theoretical uncertainty for f_2 in these regions (to an estimated σ = 20% - 30% in the difficult near-edge regions) and this appears to reduce the error of this approach to less than one standard deviation.

In regions above edges, the uncertainty in f_2 of this work and that of Chantler (1995) reduces to an estimated 1%. This is also the typical uncertainty quoted by other theoretical work, yet discrepancies between these often exist at the 6% level. Uncertainties in f_1 are dominated by small errors or sharp discontinuities in f_2. Therefore, the precision of local structure in f_1 remains uncertain, as listed in Table II. In all cases, uncertainties are quoted as percentages of $f'=f_1-Z_{eff}$, as this is the computed quantity. Near high-energy asymptotes, the accuracy of f_1 may therefore be very good, as explained in the previosu section.

Future experimental and theoretical work holds the prospect of addressing many of the issues raised in this work. The tabulation presented here resolves many of the difficulties encountered with previous tabulations, while some aspects remain to be treated in greater depth in the future, perhaps including aspects of collective behaviour and near-edge smoothing. There also appears to be a high priority for a comprehensive recalculation of scattering factors based on the approach of this work.

For general application, the tabulation presented here should be combined with Chantler (1995)[16] and may make use of scattering coefficients contained in Hubbell and Øverbø[13] (σ_{coh}), and Hubbell et al.[12](σ_{incoh}), for example.

11. Acknowledgements

We would like to thank J. H. Hubbell, E. Saloman and R. D. Deslattes in particular for their helpful interactions and promptings towards this research; and also to P. J. Mohr, M. Berger and J.-L. Staudenmann at NIST, and D. C. Creagh for their comments, support and encouragement.

12. References

[1] Chantler C. T. (1993) 'Improvements in computation of form factors,' Rad. Phys. & Chem. 41 759-766.

[2] Hubbell, J.H., Gimm, H.A. and Øverbø, I. (1980), 'Pair, triplet and total atomic cross sections (and mass attenuation coefficients) for 1 MeV – 100 GeV photons in elements Z=1 to 100,' J. Phys. Chem. Ref. Data 9, 1023-1147.

[3] Ashcroft, N. W., Mermin, N. D., ``Solid State Physics," p629 et seq. (Saunders College, Philadelphia 1976).

[4] Creagh D.C. and Hubbell J.H. (1995) 'X-ray absorption (or attenuation) coefficients,' section 4.2.4, pp189-206, in "International Table for X-ray Crystallography, Vol. C," A.J.C. Wilson, Ed. (Kluwer Academic).

[5] Chantler, C. T., J. Appl. Cryst. 25(1992) 674-693.

[6] Henke, B. L., Lee, P., Tanaka, T. J., Shimabukuro, R. L., Fujikawa, B. K., At. Dat. Nucl. Dat. Tab. 27 (1982) 1-144.

[7] Caticha, A., SPIE Proc. 1740 (1992) 81-94; Caticha, A., Phys.Rev. B47 (1993) 76.

[8] Pedulla, J., Bartos, A., Deslattes, R. D. in Physics of X-ray Multilayer Structures 1994, Technical Digest series 6 (OSA, washington DC) 31.

[9] Parratt, L. G., Phys. Rev. 95 (1954) 359-369.

[10] Berant, Z., Moreh, R., Kahane, S., Phys. Letts 69B (1977) 281-283.

[11] Ericson, T. E. O., Hüfner, J., Nucl. Phys. B57 (1973) 604-616.

[12] Hubbell J.H., Veigele Wm.J., Briggs E.A., Brown R.T., Cromer D.T., Howerton R.J. (1975), 'Atomic form factors, incoherent scattering functions, and photon scattering cross sections,' J.Phys.Chem.Ref.Data 4, 471-538.

[13] Hubbell J.H., Øverbø I. (1979), 'Relativistic atomic form factors and photon coherent scattering cross sections,' J.Phys.Chem.Ref.Data 8, 69-105.

[14] Schaupp D., Schumacher M., Smend F., Rulhusen P., Hubbell, J.H. (1983) 'Small-angle Rayleigh scattering of photons at high energies: Tabulations of relativistic HFS modified atomic form factors,' J.Phys.Chem.Ref.Data 12, 467-512.

[15] Cohen, E. R., Taylor, B. N., Rev. Mod. Phys. 59 (1987) 1121-1148.

[16] Chantler C.T. (1995) J. Phys. Chem. Ref. Data 24, 71-643.

[17] Creagh D.C. and McAuley W. (1995), 'X-ray dispersion corrections,' section 4.2.6, pp206-222, in "International Table for X-ray Crystallography, Vol. C," A.J.C. Wilson, Ed. (Kluwer Academic).

[18] Kane, P. P., Kissel, L., Pratt, R. H., Roy, S. C., Phys. Rep. 140 (1986) 75-159.

[19] Schaupp, D., Schumacher, M., Smend, F., Rulhusen, P., Hubbell, J.H., J. Phys. Chem. Ref. Data 12 (1983) 467-512.

[20] Kissel, L., Pratt, R.H., Roy, S.C., Phys.Rev. A22 (1980) 1970-2004.

[21] Pratt, R. H., Kissel, L., Bergstrom, Jr, P. M., in ''Resonant Anomalous X-ray Scattering, Theory and Applications," G. Materlik, C. J. Sparks, K. Fischer (eds) (Elsevier, North-Holland, 1994) pp9-33.

[22] Cromer, D. T., Liberman, D., J. Chem. Phys. 53 (1970) 1891-1898.

[23] Cromer, D. T., Liberman, D., Los Alamos internal report LA-4403 UC-34 (1970) 163 pages.

[24] Cromer, D. T., Mann, J. B., Acta Cryst. A24 (1968) 321-324.

[25] Cromer, D. T., Liberman, D. A., Acta Cryst. A37 (1981) 267-268.

[26] Berestetskii, V.B., Lifshitz, E. M., Pitaevskii, L.P., pp247 et seq., in "Quantum Electrodynamics" (Pergamon, Oxford, 1982).

[27] Akhiezer, A.I., Berestetsky, V.B., in "Quantum Electrodynamics" (TESE, Oak Ridge, Tennessee, 1957)

[28] Scofield J.H. (1973), 'Theoretical photoionization cross sections from 1 keV to 1500 keV,' LLNL Report UCRI-51326

[29] Saloman, E.B., Hubbell, J.H., 'X-ray Attenuation Coefficients (Total Cross Sections): Comparison of the Experimental Data Base with the recommended values of Henke and the theoretical values of Scofield for energies between 0.1-100 keV,' (1986) NBSIR 86-3431

[30] Brennan S. and Cowan P. L. (1992) 'A suite of programs for calculating x-ray absorption, reflection, and diffraction performance for a variety of materials at arbitrary wavelengths,' Rev. Sci. Inst. 63, 850-853.

[31] Chantler C.T. (1994) "Towards improved form factor tables", pp61-78 in "Resonant Anomalous X-ray Scattering Theory and Applications," G. Materlik, C.J. Sparks, K. Fischer (Eds) (Elsevier).

[32] Henke B. L., Davis J. C., Gullikson E. C., Perera R. C. C. (1988), 'X-ray interactions: Photoabsorption,

scattering, transmission and reflection at E=50-30000 eV, Z-1-92' Lawrence Berkeley Laboratory Report LBL-26259 UC-411, 376 pages.

[33] Henke B. L., Gullikson E. C., Davis J. C. (1993), 'X-ray interactions: Photoabsorption, scattering, transmission and reflection at E=50-30000 eV, Z-1-92' At.Dat.Nucl.Dat.Tables 54 181-342

[34] Saloman E.B., Hubbell J.H., Scofield J.H. (1988) 'X-ray attenuation cross sections for energies 100 eV to 100 keV and elements Z=1 to Z=92,' At.Dat.Nucl.Dat.Tables 38 1-197

[35] Cullen D.E., Hubbell J.H., Kissel L. (1997) 'EPDL97: The evaluated photon data library' Lawrence Livermore National Library Report UCRL-50400 Vol 6 Rev 5.

[36] Hubbell J.H. (1999), 'Review of photon interaction cross section data in the medical and biological context,' Physics in Medicine and Biology 44 (in press). NEW REF

[37] Bethe H.A. & Salpeter, E.E., 'Quantum mechanics of one- and two- electron atoms,' (Plenum, New York 1977).

[38] Azuma, Y., Berry, H.G., Gemmell, D.S., Suleiman, J., Westerlind, M., Sellin, I.A., Woicik, J.C., Kirkland, J.P., Phys. Rev. A51 (1995) 447-453.

[39] Hino, K., Phys.Rev. A47 (1993) 4845.

[40] Anderson, L.R., Bergdörfer, J., Phys.Rev.Lett. 71 (1993) 50.

[41] Cooper, J.W., Rad.Phys.Chem. 47(1996) 927-934.

[42] Samson, J.A.R., He, Z.H., Yin, L., Haddad, G.N., J.Phys.B27 (1994) 887.

[43] Viegele, W.S., At.Dat.Nucl.Dat.Tables 5 (1973) 51.

[44] Berkowitz, J., J.Phys.B30 (1997) 881.

[45] Chantler C.T., Barnea Z., Tran C., Tiller J., Paterson D. (1999) "Precision X-ray optics for fundamental interactions in atomic physics, resolving discrepancies in the X-ray regime," Opt Quantum Elect. (in press)

[46] Zhou B., Kissel L., Pratt R.H. (1992) 'Near-threshold structures in anomalous scattering factors,' Phys Rev A45 2983-2988.

[47] Sandiago, Umesh, T.K., Gowda, R., Pramana – J. Phys. 48 (1997) 1077-1090.

[48] Jonsson, E., Dissertation, Uppsala (1928); Cooke, B.A., Stewardson, E.A., Br. J. Appl. Phys. 15 (1964) 1315-1319; Khan, J.M., Potter, D.L., Worley, R.D., Phys.Rev. 134 (1964) A316-A320; Hughes, G.D., Woodhouse, J.B., pp202-209 in 'X-ray Optics and Microanalysis, Castaing, Deschamps, Philibert, eds (Hermann, Paris, 1966); Hon, P.K., Heinrich, K.F.J., referenced in Ref. 31 (1968); Ortner, B., Ebel, H., Linl, F., Mikrokim.Acta Suppl. IV (1970) 270-279; Kyser, D.F., Proc. 6th Int. Conf. On X-ray Optics and Microanalysis (Osaka 1971) Univ. Tokyo Press (1972) 147-156; Hemidy, A., de Thy, B., Analusis 8 (1980) 138-141.

[49] Wuilleumier F. (1972), 'Determination of mass-attenuation coefficients in krypton and xenon by

continuous analysis between 8 and 0.8 keV,' Phys. Rev. A6, 2067-2077 and refs therein.

[50] Bouldin, C. E., private communication (1994); Sorensen, L.B., Cross, J.O., Newville, M., Ravel, B., Rehr, J.J., Stragier, H., Bouldin, C.E., Woicik J.C. (1994) pp389-420 in "Resonant Anomalous X-ray Scattering Theory and Applications," G. Materlik, C.J. Sparks, K. Fischer (Eds) (Elsevier).

[51] Jensen, M. S., Phys. Lett. A74 (1979) 41.

[52] Creagh, D., NIM A295 (1990) 417-434.

[53] Maslen, E. N., Fox, A. G., O'Keefe, M. A., section 6.1.1, in International Tables for X-ray Crystallography, Vol. C, ed. A. J. C. Wilson (Kluwer Academic, Dordrecht, 1995).

[54] Chantler, C. T., J. Appl. Cryst. 25(1992) 694-713.

[55] Taupin, D., Bull.Soc.Fr.Minerál Cristallogr. 87 (1964) 469-511.

[56] Takagi, S., J.Phys.Soc.Japan 26 (1969) 1239-1253.

[57] Caticha, A., Phys. Rev. B52 (1995) 9214-9223.

[58] Batterman, B.W., Cole, H., Rev.Mod.Phys. 36 (1964) 681-717.

[59] James, R.W., Solid State Phys. 15 (1963) 53-220.

[60] International Tables for X-ray Crystallography, Vol. C, ed. A. J. C. Wilson (Kluwer Academic, Dordrecht, 1995).

[61] Berkowitz, J., J.Phys.B30 (1997) 583-592.

[62] Barkyoumb, J. H., Smith, D. Y., Phys. Rev. A41 (1990) 4863-4866.

[63] Barkyoumb, J. H., Morrison, T. I., Smith, D. Y., Phys. Letts A143 (1990) 462-466.

[64] Soufli, R., Gullikson, E.M., Appl. Optics 37 (1998) 1713-1719.

[65] Dalgarno, A., Lynn, N., Proc. Roy.Soc. London 76 (1957) 802.

[66] Klein, O., Nishina, Y., Z. Physik 52 (1929) 853-868.

[67] McMaster, W.H., Kerr del Grande, N., Mallett, J.H., Hubbell, J.H., Lawrence Livermore National Laboratory Report UCRL-50174 (1969) S2.

[68] Bearden, J. A., Rev. Mod. Phys. 39 (1967) 78-124; Bearden, J. A., Burr, A. F., Rev. Mod. Phys. 39 (1967) 125-142.

[69] Cowley, J.M., section 4.3.1 in International Tables for X-ray Crystallography, Vol. C, ed. A. J. C. Wilson (Kluwer Academic, Dordrecht, 1995).

[70] Allen, L.J., Josefsson, T.W., Phys.Rev.B52 (1995) 3184-3198.

[71] See references in Creagh, D.C., Indian J. Phys. 67B (1993) 511-525.

[72] Kissel, L., Pratt, R.H., Acta Cryst. A46 (1990) 170-175.

13. Explanation of Tables and Tabulated Figures[†]

The Tables follow a consistent grid. The figures are adapted to highlight the region of energy affected for each element, and hence vary with the atomic number.

Z	Atomic number	f_{NT}	Nuclear Thomson correction to Re(f) following equation 4 and Refs 10,11
E	Energy in keV	f_2, K-shell	Component of f_2 relating to the isolated K-shell orbital
λ	Equivalent wavelength using E. λ = 1.23984244 keV-nm, from Ref. 15	$[\mu/\rho]_{PE}$ = σ_{PE}/uA	mass attenuation coefficient in cm^2/g (see equation 8)
Atomic weight	g/mol, used in determination of conversion factors	$[\mu/\rho]_{PE,K}$	Component of μ relating to the isolated K-shell orbital (cm^2/g)
ρ	Nominal density in typical elemental material for determination of linear absorption coefficents $\mu = [\mu/\rho]\rho$	σ/ρ (coh+inc)	Estimate of coherent and incoherent = $\sigma_{coh} + \sigma_{incoh}$ scattering cross-section sum (in cm^2/g)
$\tau_{PE}=\sigma_{PE}$	atomic photoabsorption cross-section in barns/atom	Full lines on plots	Current theoretical tabulation for f_1, f_2
Edge energies	Values taken from Ref. 68	+	Earlier theoretical implementation[16] showing limited convergence near selected edges
Edge labels	Spectroscopic notation (K = 1s, L_I = 2s, L_{II} = $2p_{1/2}$, et seq.)	Thick dashes	Henke et al., experimental synthesis (Refs 32,33)
f_1, f_2	Atomic form factors in eu (electrons/atom) for forward scattering following equations 4, 7.	Dotted curves with crosses	Theoretical results for comparison reinterpolated from Refs 28,29,34, for f_2 and $[\mu/\rho]$
f_{rel}	Relativistic correction to Re(f), following Ref. 6 (denoted H82),and Refs 22-25 scaled as in Refs 16,17,52 (denoted 3/5CL)	Circles with error bars	Experimental results, summarised in Ref. 34

TABLE I: Summary of particular uses of these tables (this work and Chantler, 1995)

Form factors for forward scattering	§8.1	Direct use or interpolation, with Eqn 4
Form factors for significant momentum transfers	§8.2	Eqns 4 and 5 or Refs 13, 14, 29 or 53
Calculation of structure factors	§8.3	As §8.2 but also Eqn 1
Refractive indices	§8.3	As §8.2 but also Eqn 2
Crystallography (diffraction)	§8.4	As §8.3 but also see text for references
Multilayer reflectivity, transmission	§8.4	As §8.2 and 3 but also see text for references
Electron density studies	§8.5	As §8.3 but also Eqn 11

[†] Note the symbols used here are slightly different from Chantler, 1995, in order to clearly differentiate the mass attenuation coefficients from the atomic cross-sections and the linear absorption coefficients, but the meanings are identical.

Sum rules	§8.6	As §8.2 but also see text for references
Computation of scattering processes	§8.7	As §8.2 but also Eqs 12, 14, 1, 16, 17, 18, and (limited) Eqs 13 & 15 (see text)
Photoelectric cross-sections, linear absorption coefficient, or mass absorption coefficients	§8.8	Direct use or interpolation, with conversion as given in table headers as needed
X-ray Attenuation [Medical imaging, transmission studies]	§8.8	Direct use of total mass attenuation coefficient for Raleigh scattering
X-ray Attenuation studies with alternate scattering estimates	§8.8	Direct use of mass absorption coefficient, with Eqn 19 and possibly Refs 2,13,29
X-ray Attenuation of crystalline samples	§8.8	Direct use of mass absorption coefficient, with Eqn 19 and §8.7
Angle-dependent scattering processes	§8.8	Not applicable in general – see text
High-energy attenuation, above 100 keV	§8.9	Direct use of mass absorption coefficient, with Eqs 19,8 and possibly Refs 2,12,13,29
High-energy (γ-ray) attenuation, above 1 MeV	§8.9	See Refs 12,13
VUV studies	§8.10	Directly, but with caveats and see also Ref. 33
K-shell studies & fluorescence yields	§8.11	Directly, but see text
Electron scattering	§8.14	Eqn 21, and see text

TABLE II: Summary of estimated uncertainties of current tabulation for f_1, f_2, $[\mu/\rho]_{PE}$ and μ_{PE}, and (Chantler, 1995) for other regions of Z and energy.

Regions of energy within tabulated region	Estimated typical uncertainty		
	f_2, $[\mu/\rho]_{PE}$ & μ_{PE}	f_2, $[\mu/\rho]_{PE}$ & μ_{PE}	f'
0.001 eV – 1 MeV	MONATOMIC GASES	SOLIDS, LIQUID	f_1-Z (see §9)
Below 200 eV [correlations, phonons]	50%-100%[33]	100%-200%[33]	50%-100%[33]
200 eV – 500 eV	20%-30%[33]	50%-100%[33]	20%-50%

500 eV – 1 keV	3%-10%[33]	5%-20%[33]	5%-15%
Near edges (within 0.1%)	20%-30%	50%	50%-100%
Near K edges (within 10%)	10%	10%-20%	30%
Near K edges ($1.1 < E/E_K < 1.2$)	3%	3%	10%
Well above K edges ($E/E_K > 1.2$)	1%	1%	1%-2%
Near L I, M I – M III edges (within 15%)	15%	15%-30%	30%
Near L I, M I – M III edges ($1.15 < E/E_{edge} < 1.4$)	4%	4%	10%
Well above L I, M I – M III edges ($E/E_{edge} > 1.4$)	1%	1%	1%-2%
Near L II/III, M IV/V edges (within 15%)	20%	20%-40%	30%
Near L II/III, M IV – M V edges ($1.15 < E/E_{edge} < 1.4$)	4%	4%	10%
Well above L II/III, M IV – M V edges ($E/E_{edge} > 1.4$)	1%	1%	1%-2%
Above 200 keV (see also §5 & §8.9)	2% -3%	2% -3%	1%-2%

TABLE III: Form factors, attenuation and scattering cross-sections, Z=30-36, from E=0.9 keV to E=6 keV.

[Insert and format file FT99.dat3036]

TABLE IV: Form factors, attenuation and scattering cross-sections, Z=61-88, from E=0.9 keV to E=10 keV.

[Insert and format files FT99.dat6074 and FT99.dat7589]

Figure Captions:

Fig. 1. Imaginary component of the atomic form factor for hydrogen, following a variety of models. Henke et al.3233 covers a more restricted energy range, and the Sauter formula (e.g. Ref.37) only becomes a useful approximation at energies above 40

keV. With these two exceptions, all approaches appear very similar across several decades of energy and form factor. The Chantler result is accurate to within approximately 2% up to 300 keV for an isolated hydrogen atom.

Fig. 2. Attenuation in He. Experimental data from Azuma et al. (1995). Chantler (1995) (full line and dash-with-cross) agrees with experiment, as compared to Scofield unrenormalised (dash-dot-dot-dot) or renormalised (short dash, Saloman, Hubbell and Scofield, 1988). Uncertainty in scattering (which dominates above 11 keV) is indicated by variation between line and dash-with-cross. Scattering component in the dash-with-cross curve is derived from Saloman, Hubbell and Scofield, 1988, in turn from Brown in Hubbell et al., 1975.

Fig. 3. Attenuation in Cu (Z=29), represented by Im (f) = f_2. [μ/ρ] (in cm^2/g) = f_2 (e/atom) x 6.62202 $x10^5$. Experimental data from Saloman, Hubbell and Scofield (1988). Chantler (1995), Scofield theory and even the smoothed structure of Henke (1988) agree within uncertainties of available experiment. In this case, the qualitative near-edge structure is the same for all tabulations, except for the apparent omission of the L_{III} edge in the Henke curve.

Fig. 4. Attenuation in Zn (Z=30), represented by Im (f) = f_2. [μ/ρ] (cm^2/g) = f_2 (e/atom) x $6.43627x10^5$. Experimental data from Saloman, Hubbell and Scofield (1988). Chantler (1995), Scofield and Henke (1988) agree with available experiment, but all have large error, as indicated by the 'New Result.'

Fig. 5. Attenuation in Zn (Z=30), represented by [μ/ρ] (cm^2/g). Experimental data from Saloman, Hubbell and Scofield (1988). Chantler (1995), Scofield and Henke (1988) agree with available experiment, but all have large error, as indicated by the 'New Result.'

Fig. 6. The real component of the form factor in Zn (Z=30), represented by f_1 (e/atom). This is responsible for scattering, so that accurate computations of coherent and incoherent scattering, including Bragg-Laue or TDS extremes, should make use of this coefficient. This plot illustrates the effect of the wavefunction imprecision on the structure of Re (*f*). The 'New Result' improves upon the qualitative structure given by Chantler (1995) and by Henke (1988).

Fig. 7. Attenuation in Pm (Z=61), represented by Im (*f*) = f_2. $[\mu/\rho]$ (cm^2/g) = f_2 (e/atom) x 2.90209×10^5.Experimental data from Saloman, Hubbell and Scofield (1988). The extended range plotted shows the insignificance of Rayleigh scattering for all but the highest energies plotted (where the contribution reaches 1%). The lower energy behaviour illustrates the increasing uncertainty at lower energies. The near-edge structure of the 'New Result' follows qualitative expectations unlike all others shown.

Fig. 8. The result of figure 4 presented as a percentage deviation of tabulated results for f_2 compared to this work, for Zinc. All results show large excursions from the reference line, and all have corresponding imprecision in this near-edge region. The result of Henke (1988) is relatively smooth.

Fig. 9. The result of figure 7 presented as a percentage deviation of tabulated results for f_2 compared to this work, for Z=61. All results show large excursions from the reference line, and all have corresponding imprecision in this near-edge region.

Fig. 10. The best experimental data in the range of Z=30-36, for Kr Z=36 (Wuilleumier, 1972), supports this work in structure and detail. Im (*f*) = f_2. The experimental values include contributions from scattering. $[\mu/\rho]$ (in cm^2/g) = f_2 (e/atom) x 5.02152×10^5.

Fig. 11. A confirmation that this discrepancy is insignificant for f_1 in Rb (Z=37) and hence that we have no new result to present in this region. With the exception of the fine structure at the edge, Henke (1988) is in good agreement with Chantler (1995).

Fig. 12. A confirmation that this discrepancy is insignificant for f_2 in Rb (Z=37) and hence that we have no new result to present in this region. Hence the lower range of the tabulation is only given for Z=30 to Z=36. Theoretical and experimental uncertainties increase towards lower energies.

Fig. 13. A confirmation that this discrepancy is insignificant for f_1 in Pr (Z=59) and hence that we have no new result to present in this region. Chantler (1995) appears to give a sound prediction of the independent particle approximation, especially compared to Henke (1988).

Fig. 14. A confirmation that this discrepancy is insignificant for f_2 in Pr (Z=59) and hence that we have no new result to present in this region. Hence the upper range of the tabulation is only given for Z=60 to Z=89.

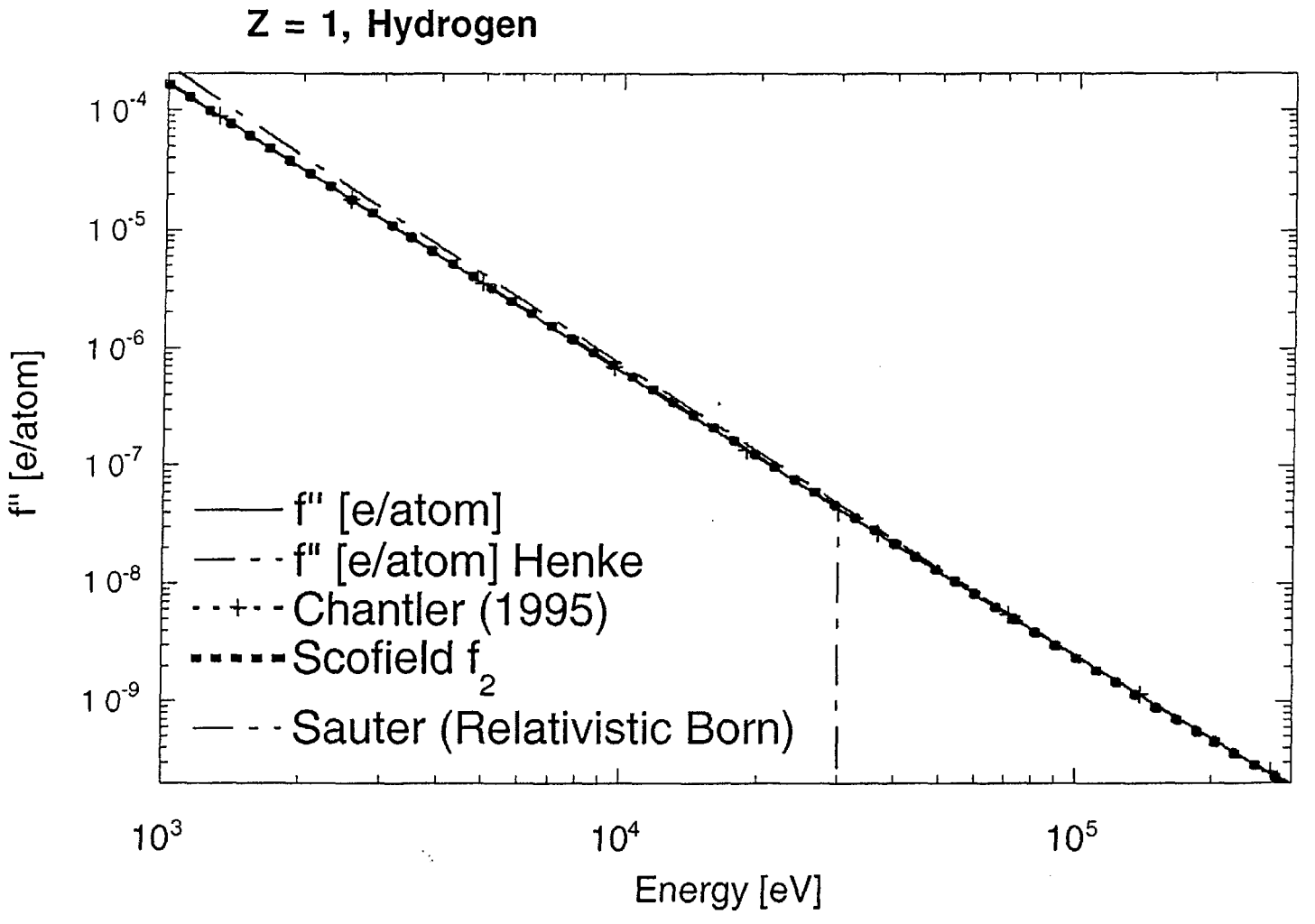
Z = 1, Hydrogen
f'' [e/atom]
1 0-4
1 0-5
1 0-6
1 0-7
1 0-8
1 0-9
f'' [e/atom]
f'' [e/atom] Henke
Chantler (1995)
Scofield f2
Sauter (Relativistic Born)
10^3
10^4
10^5
Energy [eV]

Fig. 1

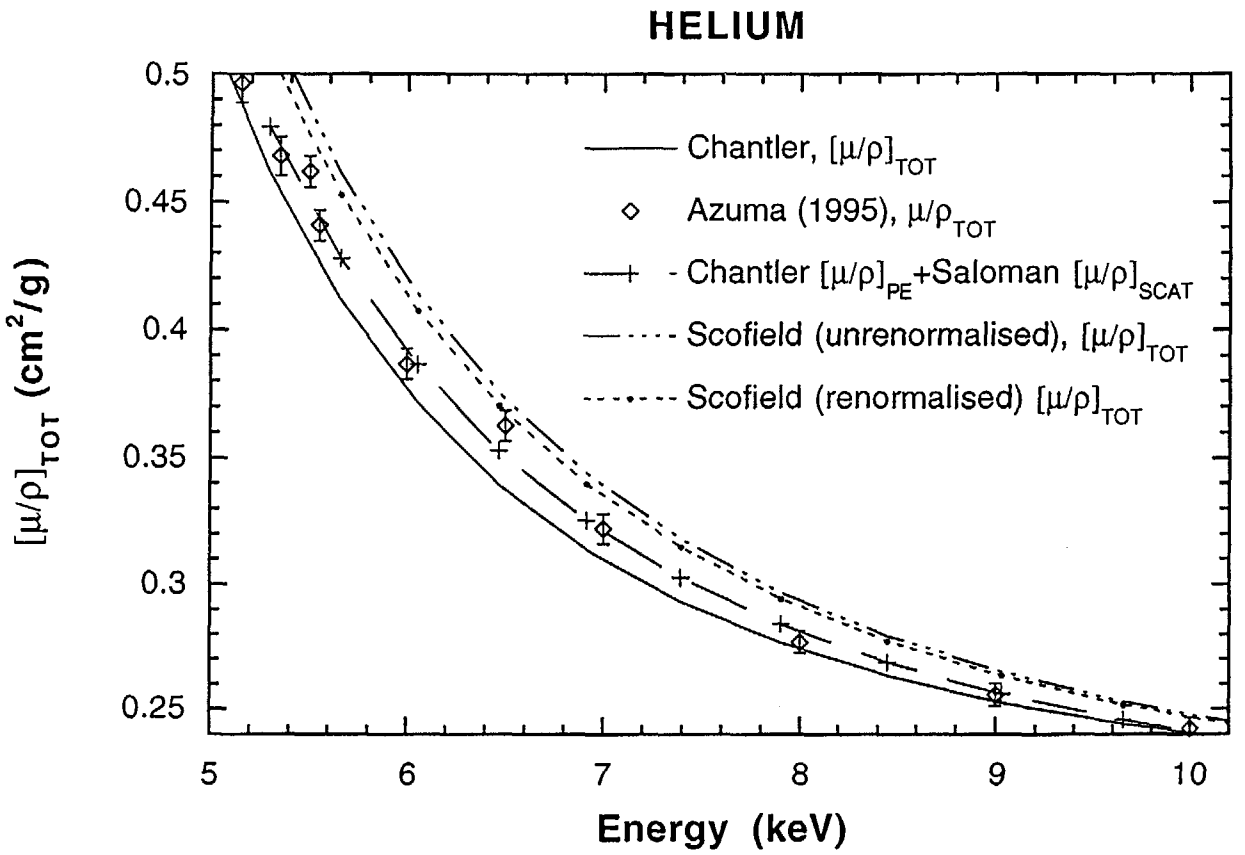
HELIUM
0.5
0.45
0.4
0.35
0.3
0.25
5
6
7
8
9
10
Energy (keV)
[μ/ρ]TOT (cm²/g)
Chantler, [μ/ρ]TOT
Azuma (1995), μ/ρTOT
Chantler [μ/ρ]PE+Saloman [μ/ρ]SCAT
Scofield (unrenormalised), [μ/ρ]TOT
Scofield (renormalised) [μ/ρ]TOT

Fig.2

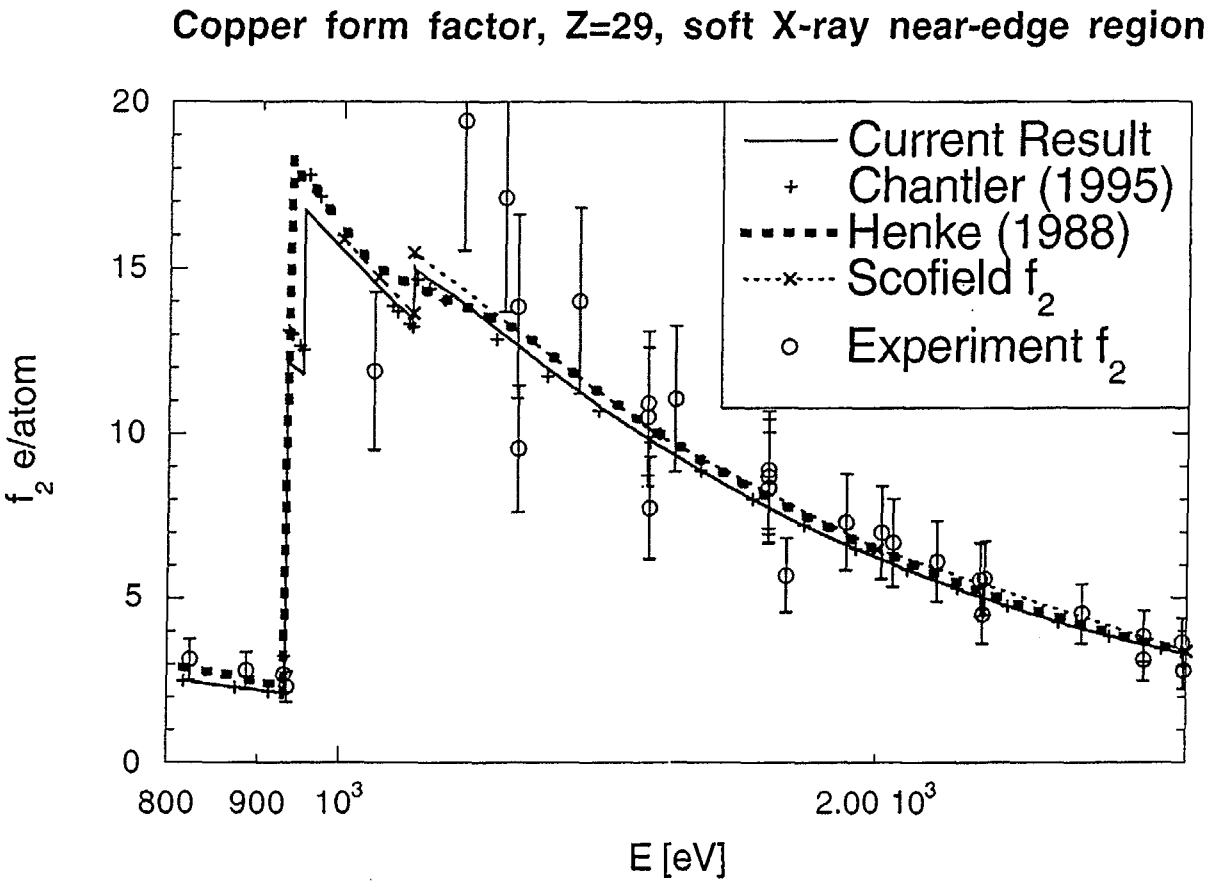
Copper form factor, Z=29, soft X-ray near-edge region
Current Result
Chantler (1995)
Henke (1988)
Scofield f2
Experiment f2
f2 e/atom
E [eV]
20
15
10
5
0
800
900
10^3
2.00 10^3

Fig.3

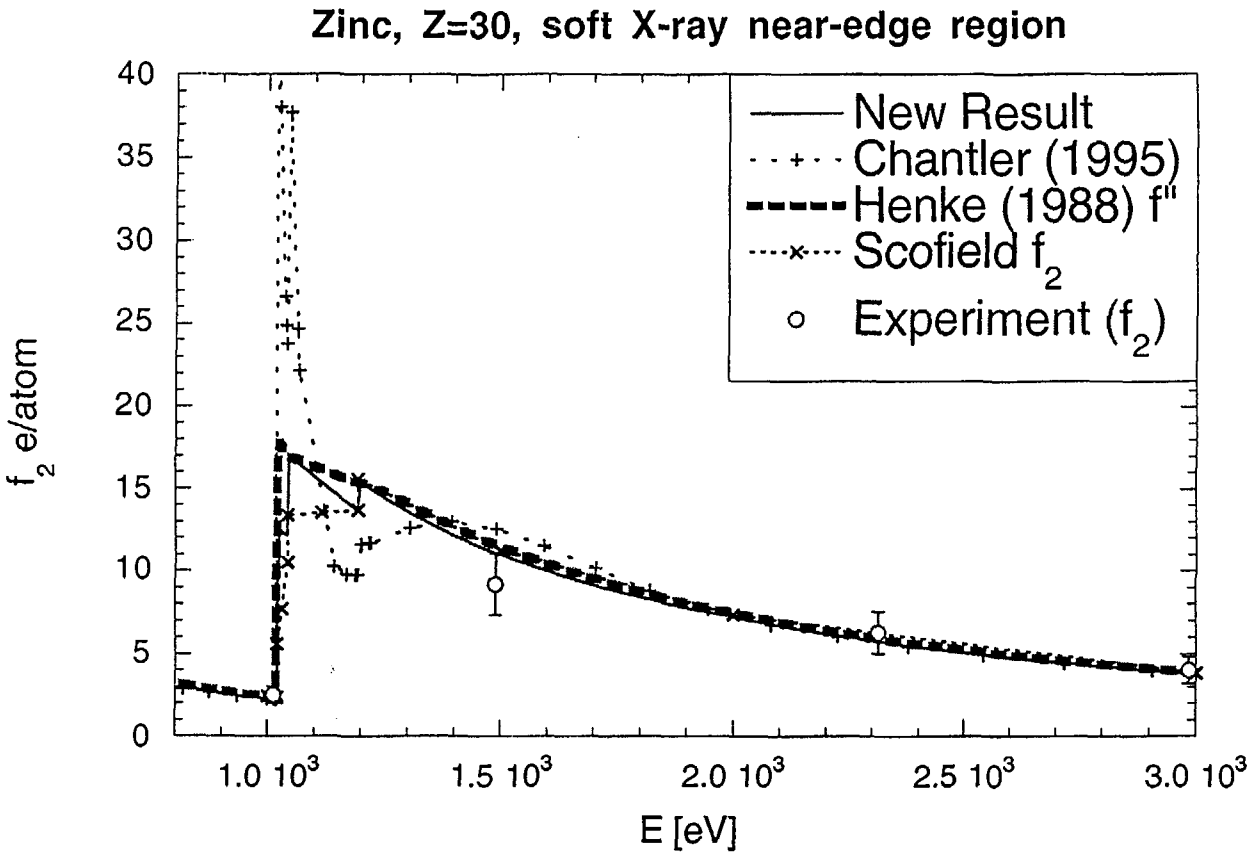
Zinc, Z=30, soft X-ray near-edge region
New Result
Chantler (1995)
Henke (1988) f''
Scofield f2
Experiment (f2)
f2 e/atom
E [eV]
0
5
10
15
20
25
30
35
40
1.0 10^3
1.5 10^3
2.0 10^3
2.5 10^3
3.0 10^3

Fig.4

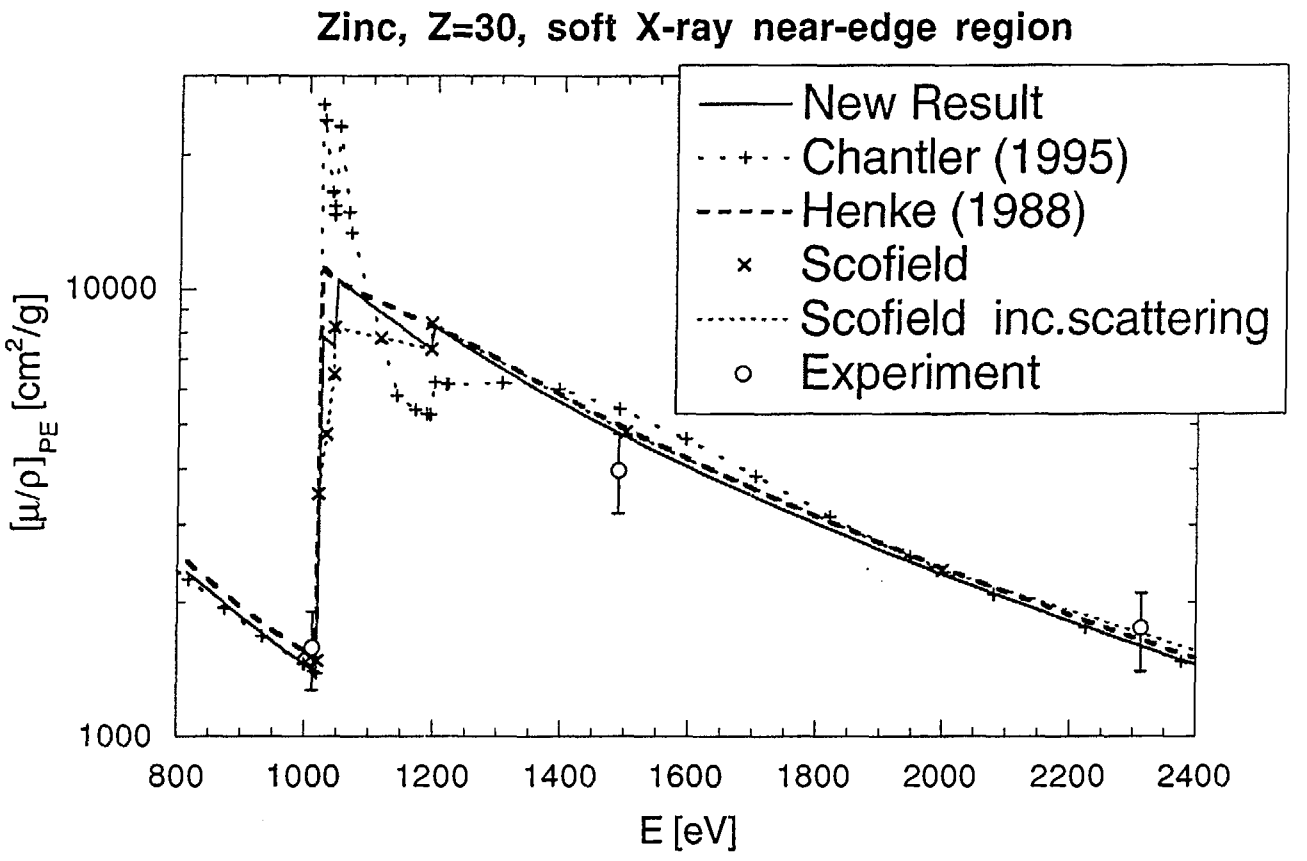
Zinc, Z=30, soft X-ray near-edge region
New Result
Chantler (1995)
Henke (1988)
Scofield
Scofield inc.scattering
Experiment
[μ/ρ]PE [cm²/g]
10000
1000
800
1000
1200
1400
1600
1800
2000
2200
2400
E [eV]

Fig.5

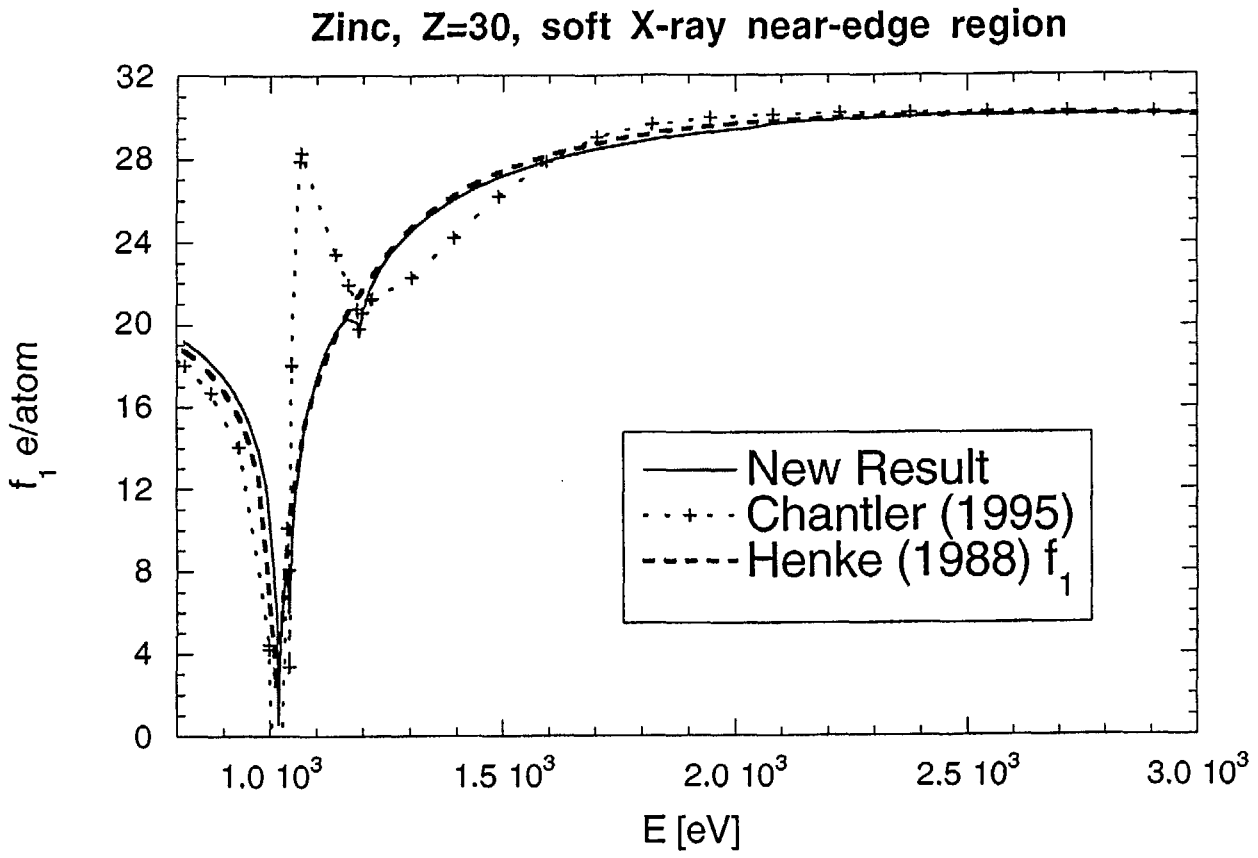
Zinc, Z=30, soft X-ray near-edge region
f1 e/atom
E [eV]
New Result
Chantler (1995)
Henke (1988) f1
0
4
8
12
16
20
24
28
32
1.0 10^3
1.5 10^3
2.0 10^3
2.5 10^3
3.0 10^3

Fig.6

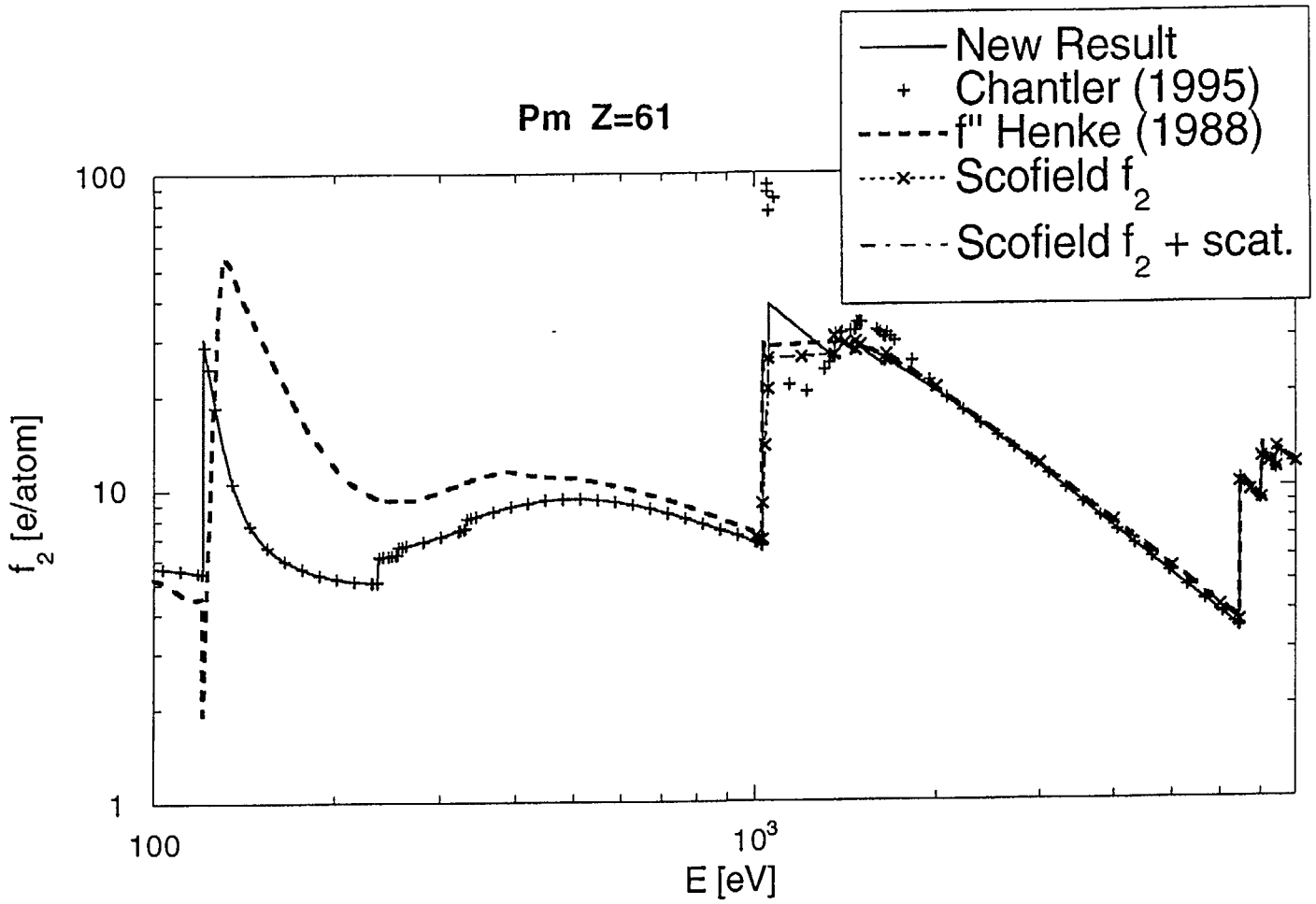
Pm Z=61
New Result
Chantler (1995)
f'' Henke (1988)
Scofield f2
Scofield f2 + scat.
100
10
1
f2 [e/atom]
100
10^3
E [eV]

Fig.7

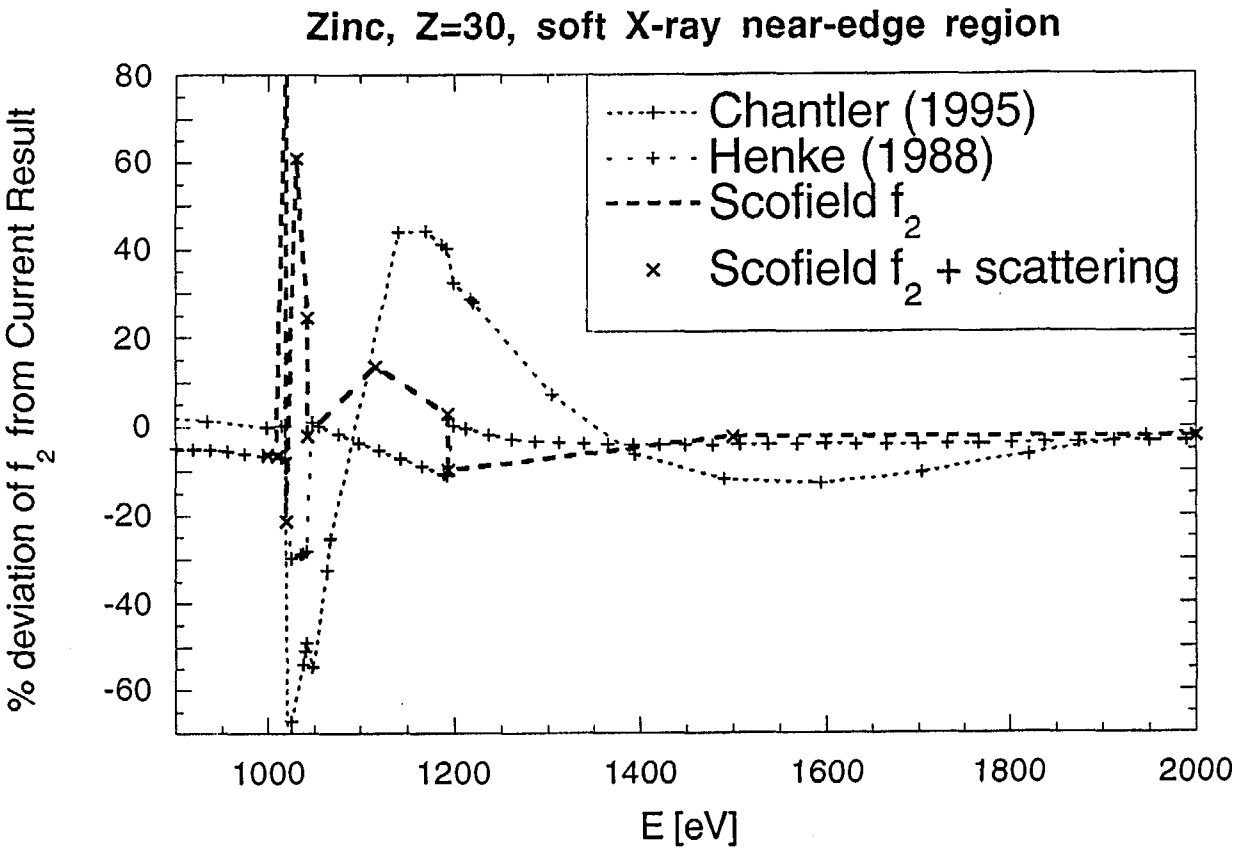
Zinc, Z=30, soft X-ray near-edge region
Chantler (1995)
Henke (1988)
Scofield f2
Scofield f2 + scattering
% deviation of f2 from Current Result
80
60
40
20
0
-20
-40
-60
1000
1200
1400
1600
1800
2000
E [eV]

Fig.8

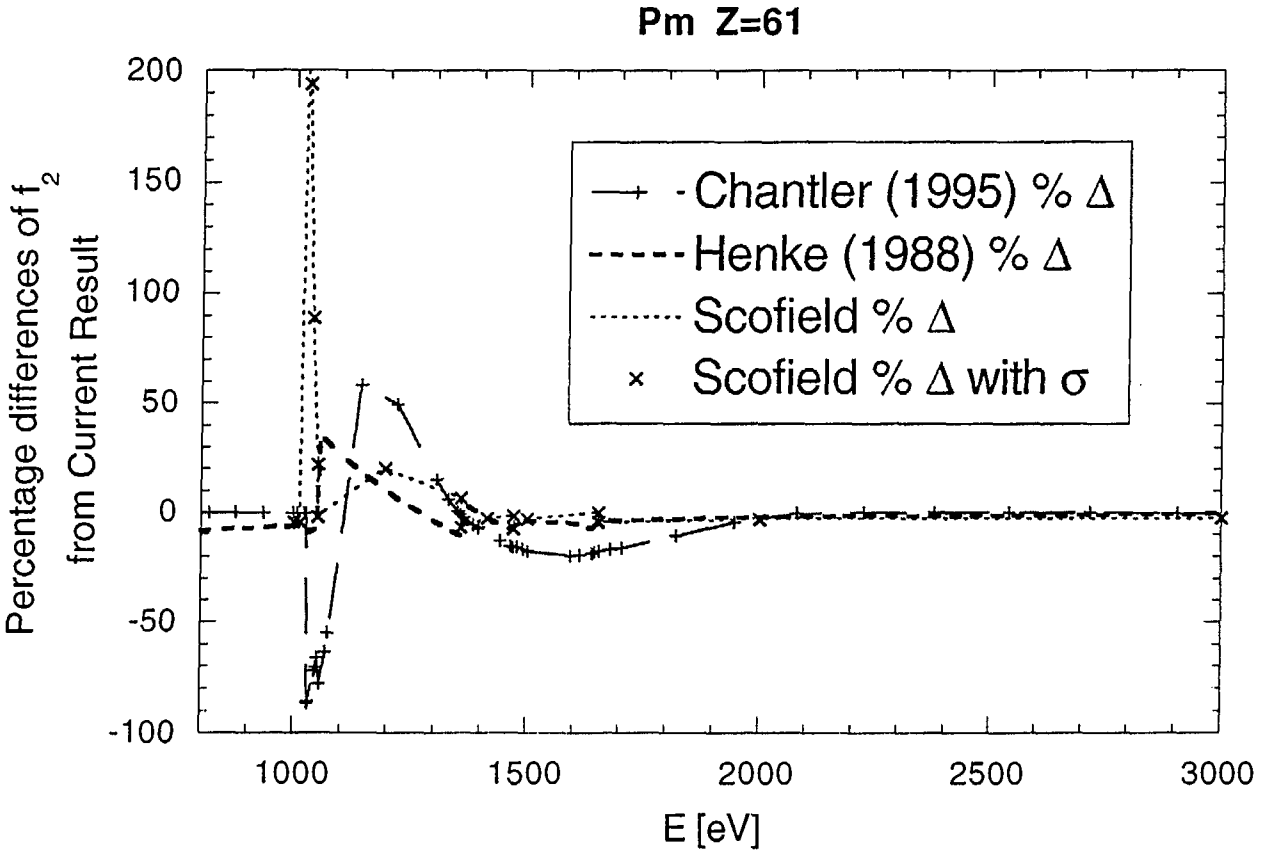
Pm Z=61
Percentage differences of f_2 from Current Result
200
150
100
50
0
-50
-100
1000
1500
2000
2500
3000
E [eV]
Chantler (1995) % Δ
Henke (1988) % Δ
Scofield % Δ
Scofield % Δ with σ

Fig.9

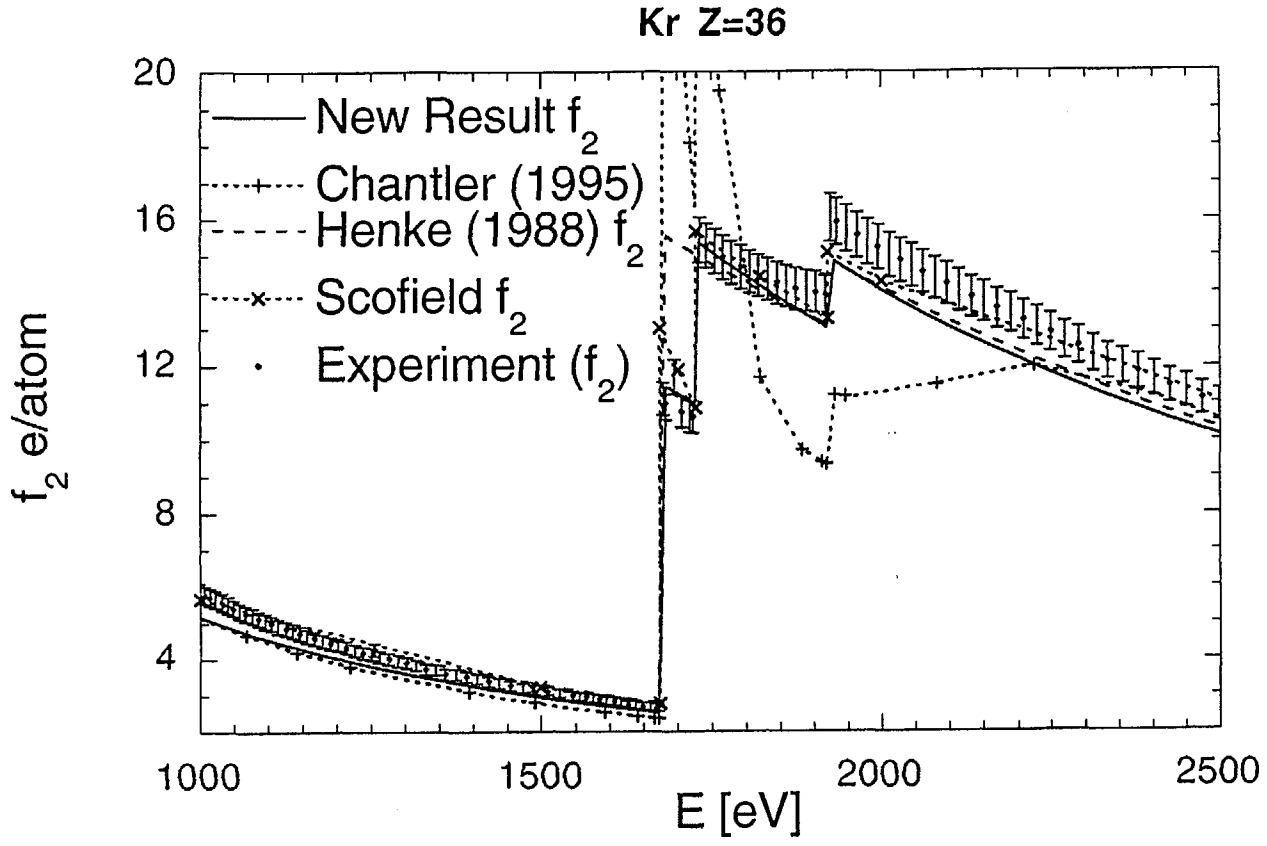
Kr Z=36
New Result f_2
Chantler (1995)
Henke (1988) f_2
Scofield f_2
Experiment (f_2)
f_2 e/atom
E [eV]
20
16
12
8
4
1000
1500
2000
2500

Fig. 10

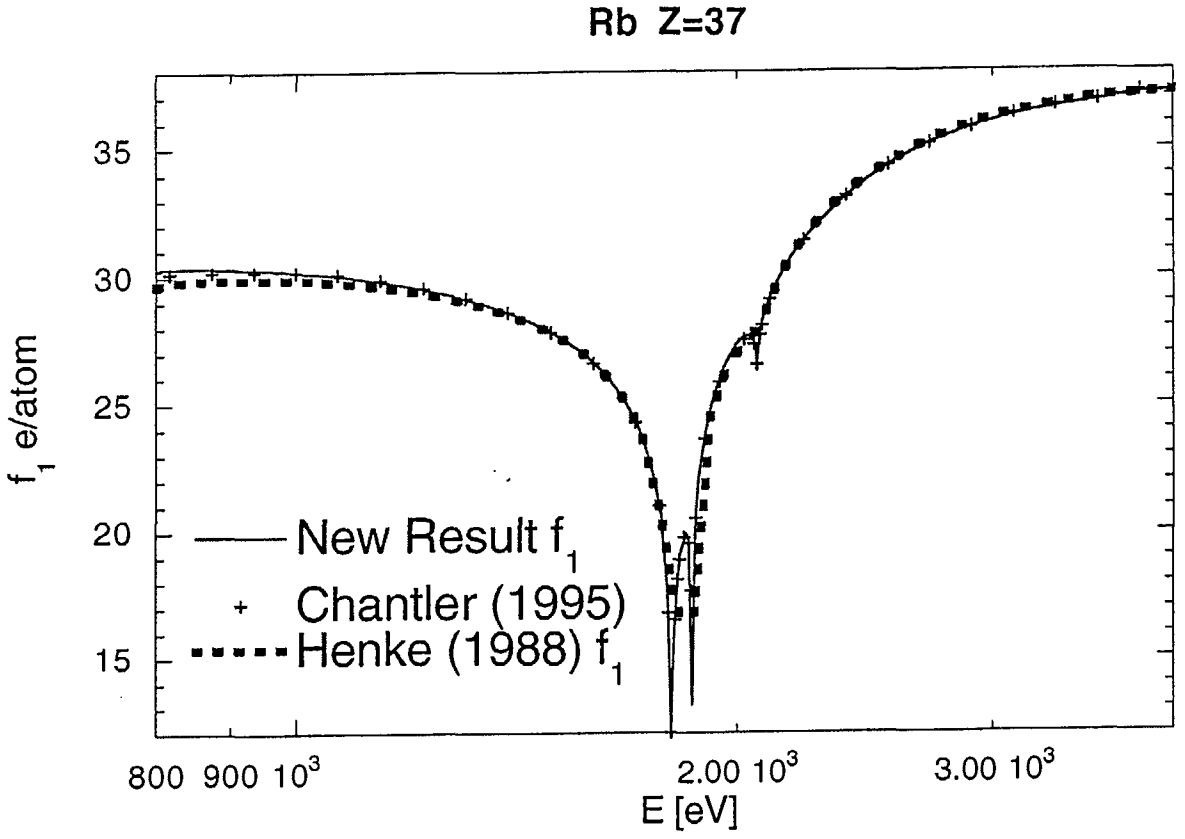
Rb Z=37
35
30
25
20
15
f1 e/atom
New Result f1
Chantler (1995)
Henke (1988) f1
800 900 10^3
2.00 10^3
3.00 10^3
E [eV]

Fig. 11

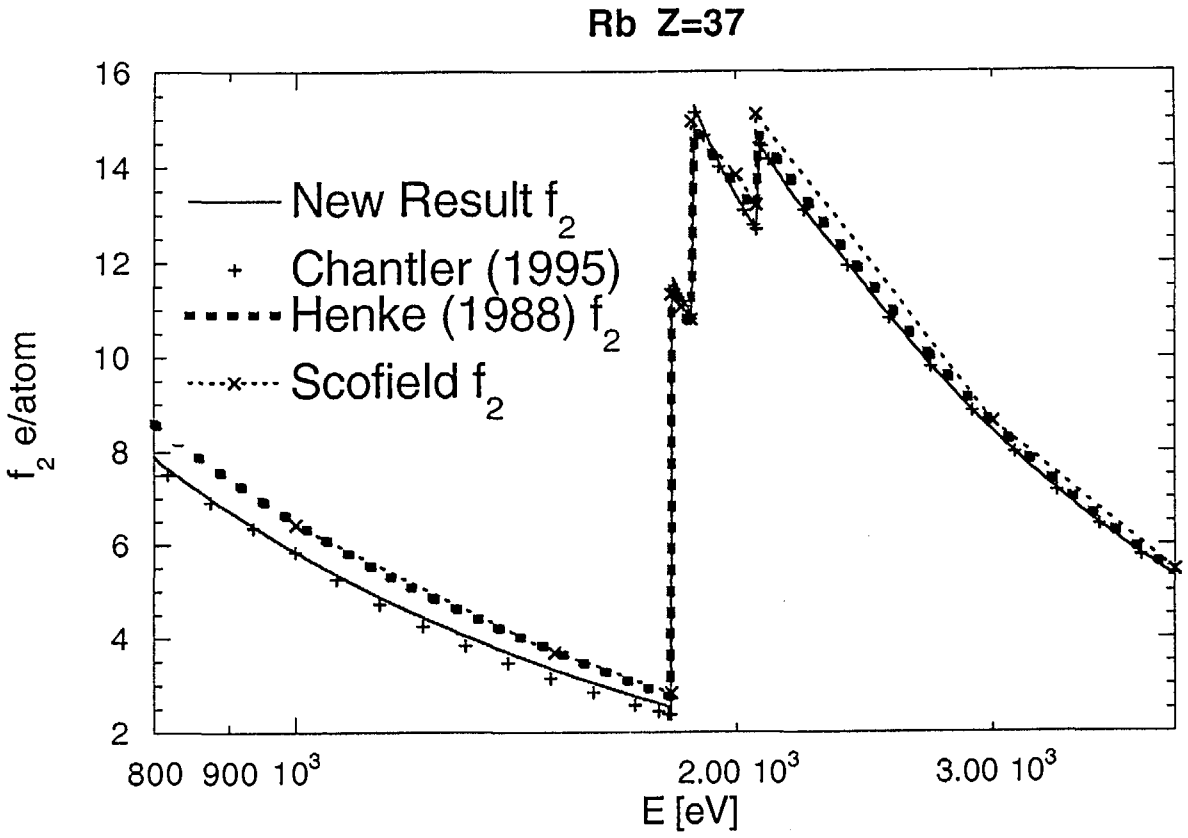
Rb Z=37
New Result f_2
Chantler (1995)
Henke (1988) f_2
Scofield f_2
f_2 e/atom
E [eV]
16
14
12
10
8
6
4
2
800 900 10^3
2.00 10^3
3.00 10^3

Fig. 12

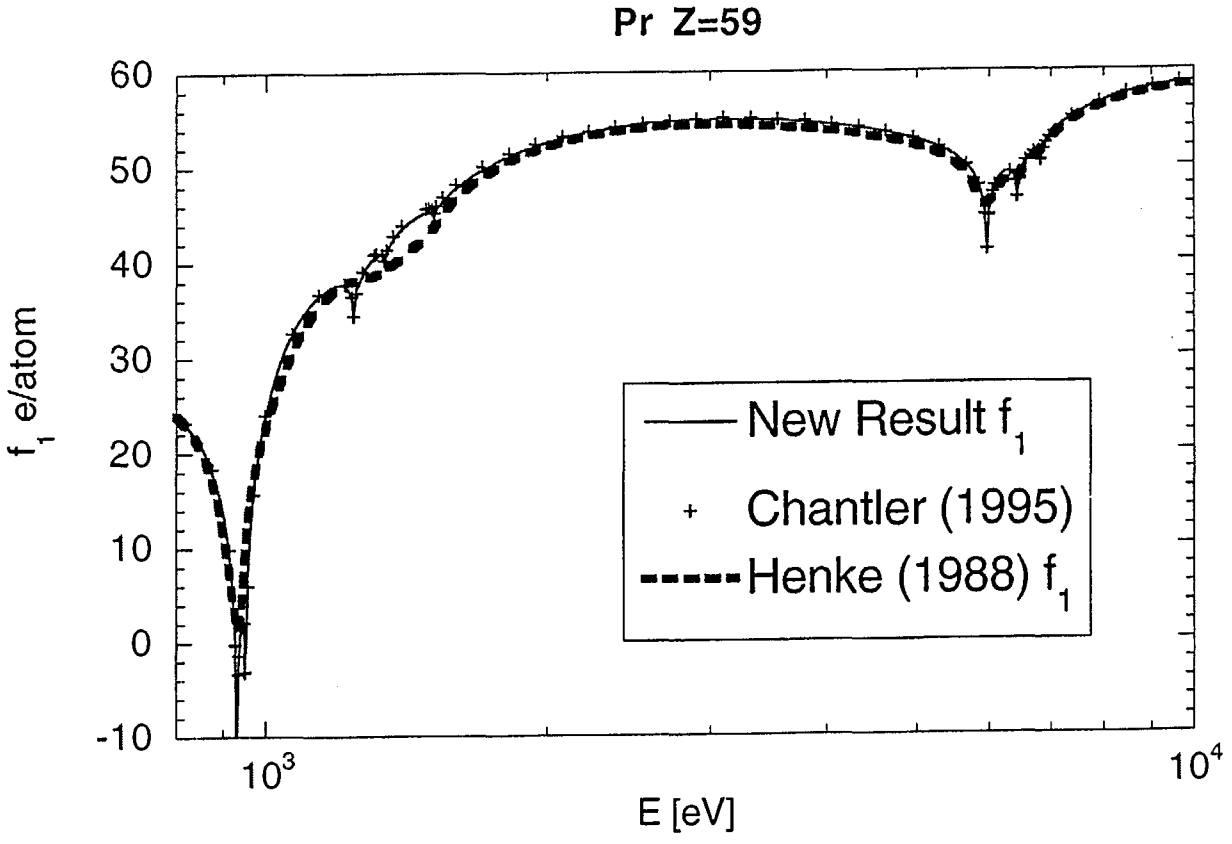
Pr Z=59
60
50
40
30
20
10
0
-10
f_1 e/atom
10^3
10^4
E [eV]
New Result f_1
Chantler (1995)
Henke (1988) f_1

Fig. 13

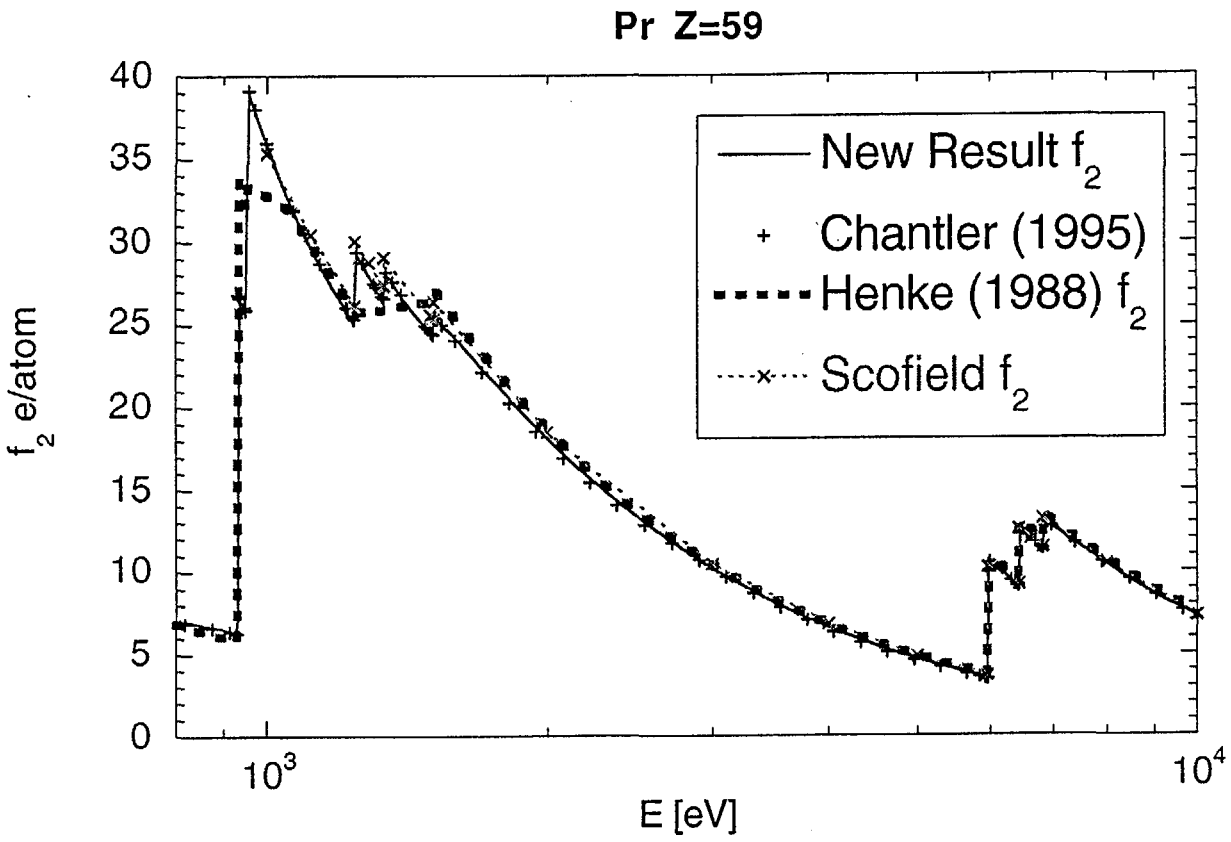
Pr Z=59
40
35
30
25
20
15
10
5
0
f_2 e/atom
10^3
10^4
E [eV]
New Result f_2
Chantler (1995)
Henke (1988) f_2
Scofield f_2

Fig. 14